



Multivariate Prediction of Total Water Storage Changes Over West Africa from Multi-Satellite Data

Ehsan Forootan, Jürgen Kusche, Ina Loth, Wolf-Dieter Schuh, Annette Eicker, Joseph Awange, Laurent Longuevergne, B. Diekkrüger, Michael Schmidt, C.K. Shum

► To cite this version:

Ehsan Forootan, Jürgen Kusche, Ina Loth, Wolf-Dieter Schuh, Annette Eicker, et al.. Multivariate Prediction of Total Water Storage Changes Over West Africa from Multi-Satellite Data. Surveys in Geophysics, Springer Verlag (Germany), 2014, 35 (4), pp.913-940. <10.1007/s10712-014-9292-0>. <insu-01060161>

HAL Id: insu-01060161

<https://hal-insu.archives-ouvertes.fr/insu-01060161>

Submitted on 13 Oct 2014

HAL is a multi-disciplinary open access archive for the deposit and dissemination of scientific research documents, whether they are published or not. The documents may come from teaching and research institutions in France or abroad, or from public or private research centers.

L'archive ouverte pluridisciplinaire **HAL**, est destinée au dépôt et à la diffusion de documents scientifiques de niveau recherche, publiés ou non, émanant des établissements d'enseignement et de recherche français ou étrangers, des laboratoires publics ou privés.

Multivariate prediction of total water storage changes over West Africa from multi-satellite data

Ehsan Forootan forootan@geod.uni-bonn.de (1) Jürgen Kusche (1) Ina Loth (1) Wolf-Dieter Schuh (1)
Annette Eicker (1) Joseph Awange (2) Laurent Longuevergne (3) Bernd Diekkrüger (4)
Michael Schmidt (5) C. K. Shum (6) (7)

1. Institute of Geodesy and Geoinformation, Bonn University, Nussallee 17, 53115, Bonn, NRW, Germany
2. Western Australian Centre for Geodesy and The Institute for Geoscience Research, Curtin University, Perth, Australia
3. Géosciences Rennes, UMR CNRS 6118, Université de Rennes1, Rennes, France
4. Hydrology and Environmental Modelling, Department of Geography, Bonn University, Bonn, NRW, Germany
5. German Geodetic Research Institute (DGFI), Munich, Germany
6. Division of Geodetic Science, School of Earth Sciences, Ohio State University, Columbus, Ohio, USA
7. Institute of Geodesy and Geophysics, Chinese Academy of Sciences, Beijing, China

Abstract West-African countries have been exposed to changes in rainfall patterns over the last decades, including a significant negative trend. This causes adverse effects on water resources of the region, for instance, reduced freshwater availability. Assessing and predicting large-scale total water storage (TWS) variations is necessary for West Africa, due to its environmental, social, and economical impacts. Hydrological models, however, may perform poorly over West Africa due to data scarcity. This study describes a new statistical, data-driven approach for predicting West African TWS changes from (past) gravity data obtained from the Gravity Recovery and Climate Experiment (GRACE), and (concurrent) rainfall data from the Tropical Rainfall Measuring Mission (TRMM) and sea surface temperature (SST) data over the Atlantic, Pacific, and Indian Oceans. The proposed method, therefore, capitalizes on the availability of remotely sensed observations for predicting monthly TWS, a quantity which is hard to observe in the field but important for measuring regional energy balance, as well as for agricultural, and water resource management. Major teleconnections within these data sets were identified using independent component analysis (ICA) and linked via low-degree autoregressive models to build a predictive framework. After a learning phase of 72 months, our approach predicted TWS from rainfall and SST data alone that fitted to the observed GRACE-TWS better than that from a global hydrological model. Our results indicated a fit of 79% and 67% for the first year prediction of the two dominant annual and inter-annual modes of TWS variations. This fit reduces to 62% and 57% for the second year of projection. The proposed approach, therefore, represents strong potential to predict the TWS over West Africa up to two years. It also has the potential to bridge the present GRACE data gaps of one month about each 162 days as well as a - hopefully - limited gap between GRACE and the GRACE follow-on mission over West Africa. The presented method could

E. Forootan
Institute of Geodesy and Geoinformation, Bonn University, Nussallee 17, D53115, Bonn, NRW,
Germany
Tel.: +49228736423
Fax: +49228733029
E-mail: forootan@geod.uni-bonn.de

also be used to generate a near-real time GRACE forecast over the regions that exhibit strong teleconnections.

Keywords Predicting GRACE-TWS · West Africa · Autoregressive model · ICA · GRACE gap filling

1 Introduction

West African climate is highly variable, ranging from tropical to semi-arid and arid over a limited 1500-km North-South gradient. The main source of precipitation over a large part of West Africa (WA) is driven by the WA monsoon system and tightly linked to large-scale pattern of ocean-atmosphere-land interaction (Gianini et al., 2003, 2008). Inter-decadal rainfall decrease over WA was highlighted as one of the largest precipitation patterns on the planet over the last half century (Ali and Lebel, 2009), leading to high risks of prolonged droughts, as in the 1970s and 1980s. Moreover, global warming adds up multiple threats to the region, with the duration and magnitude of droughts and floods expected to increase (Nicholson, 2000, Speth et al., 2011). It is of critical importance to understand and predict the impact of the WA climatic system on water resources over timescales of several months, as the livelihoods of roughly 70% of the region's population depend on uncertain rainfall and exposure to climate risk (Hansen et al., 2011).

Drought severity is classically expressed in terms of the Palmer drought index, based on moisture data only (Heim 2002). However, this index does not explicitly account for the state of all water storage compartments (Long et al., 2013), as prolonged drought conditions may have an impact on deeper groundwater systems even with limited anthropic pumping (Chen et al., 2010). Houborg et al. (2012) showed significant interest in incorporating total water storage observations (TWS), defined as the sum of all available water storage on and below the surface of the Earth, to be used for drought monitoring. Its applicability is due to the fact that TWS can represent all available forms of water resource (Scanlon et al., 2012, Schol et al., 2008), thus, might be a better representative of drought compared to soil moisture or groundwater compartment alone.

Importance of quantifying TWS variations goes beyond its application in water resource studies. In general, the internal states of storage compartments determine their reaction to imposed boundary conditions. Runoff is driven by water stored in soil compartment and groundwater systems. Soil moisture layers - and groundwater to a lesser extend - also control evapotranspiration, cooling the land surface and regulating local energy and water balances (Koster et al., 2004). In this sense, WA has been highlighted as a 'hot spot', where the land-atmosphere coupling could play an important role, through the recycling of precipitation and the modulation of rainfall gradients (Douville et al., 2006). Main processes affecting rainfall and water availability in WA at seasonal to decadal time scales have been extensively studied within the framework of international efforts under the AMMA¹ initiative (e.g. Redelsperger et al. 2006). Beside land-atmosphere coupling, WA monsoon variability coincides with other overlapping shifts like those in global temperature and natural sea surface temperature (SST) oscillations in all tropical oceans,

¹ African Monsoon Multidisciplinary Analysis

40 showing remote (Pacific) or local (Atlantic and Indian) influences (see Rodríguez-
41 Fonseca et al., 2011 and references therein, Mohino et al., 2011). Diatta and Fink
42 (2014) studied the relationships between climate indices and monsoon rainfall, de-
43 rived from rain gauge data, over West Africa, covering 1921 to 2009, and reported
44 positive correlations between Sahel rainfall and the Atlantic Multi-decadal Oscil-
45 lation (AMO), as well as the Atlantic Meridional Mode (AMM). Their results also
46 indicated a significant impact of ENSO on inter-annual variability of precipita-
47 tion over WA. Up to now, however, complex coupled ocean-atmosphere models
48 represented limited skills to accurately simulate the main SST-WA monsoon tele-
49 connections, both at inter-annual and decadal scales. This is reported to be caused
50 by the simplification of different aspects of the climate system and of persistent
51 biases (e.g., Rodríguez-Fonseca et al., 2011).

52 Land surface models (LSMs) and hydrological models are commonly applied
53 to simulate the impact of climate on storage compartments (e.g., Döll et al., 2003,
54 Rodell et al., 2004, van Dijk et al., 2013). However, the quality of the models
55 strongly depends on model structure, boundary conditions (rainfall and evapo-
56 transpiration) and data availability, and also on model calibration/parametrization
57 (Güntner et al., 2007). Over WA, modeling the impact of the monsoon on water
58 resources is restricted by limited data for calibration/validation purposes (Boone
59 et al., 2009, Schuol and Abbaspour, 2006), leading to large magnitude of uncer-
60 tainties on the water balance and TWS.

61 Time-variable gravity solution of the Gravity And Climate Experiment (GRACE)
62 mission offers an opportunity to remotely measure large-scale TWS changes on re-
63 gional and global scale (Tapley et al. 2004, Schmidt et al., 2008a). A few studies
64 have highlighted the critical interest of GRACE-TWS observations in WA due to
65 the sparse distribution of in situ observation network with respect to the size of
66 the region (Xie et al., 2012). Nahmani et al. (2012) showed that GRACE accu-
67 rately estimates the annual variability of WS over WA, when compared to the
68 output of hydrological models and GPS observations. Grippa et al. (2011) carried
69 out a model comparison study between various GRACE products and nine land
70 surface models (LSMs) and showed substantial differences between GRACE-TWS
71 and LSMs. The differences were mainly ascribed to the weakness of the LSMs to
72 correctly simulate water in surface reservoirs and evapotranspiration during the
73 dry seasons.

74 This study presents a multivariate statistical TWS forecasting approach for
75 West Africa (WA). Our goal is to capitalize on the availability of homogeneously
76 processed, remotely sensed observations of gravity from GRACE, sea surface tem-
77 perature (SST) from satellite data, as well as rainfall data from the Tropical Rain-
78 fall Measuring Mission (TRMM), and predict large-scale annual and inter-annual
79 variability of West-African TWS changes up to a few years. Therefore, the term
80 ‘prediction’ or ‘forecast’ in this study refers to estimation of the TWS quantity, for
81 the period that TWS has not been observed, using its indicators, which in our case
82 are SST and precipitation changes. A statistical approach, based on ‘system iden-
83 tification’ framework (Ljung, 1987), is chosen here for our predictions (see Section
84 3) since we are interested in accurate final monthly values of TWS rather than
85 exploring the mechanism of changes in TWS compartments (e.g., soil moisture
86 and groundwater) and their interactions. A similar concept has already been used,
87 e.g., by the USA’s National Oceanic and Atmospheric Administration (NOAA)
88 for predicting climatic parameters (<http://www.cpc.ncep.noaa.gov/>). We should

89 mention here that one could also alternatively use ‘gap-filler’ approaches (e.g.,
90 Rietbroek et al., 2014) to estimate (or predict) surface load or TWS over a re-
91 gion of interest. We will show later that the prediction approach here provides up
92 to two years TWS predictions, while retaining the spatial resolution of GRACE
93 products. Reager and Famiglietti (2013) presented an experimental predictions
94 approach that relates water storage changes to precipitation forcing and then gener-
95 alize the relation based on large-scale basin characteristics. Unlike our proposed
96 method, this approach requires extra information about basin characteristics.

97 The predictability skill of the proposed statistical approach would be optimal if
98 major physical processes over the region of study are included in the learning phase.
99 Thus, both ocean-atmosphere and land-atmosphere processes are represented as
100 predictors of West African TWS changes: (i) SST variations over the major oceanic
101 basins of the Atlantic, Pacific, and Indian Oceans (ii) TRMM rainfall observation
102 over West Africa. Although other predictors might also improve the forecasting
103 results (evapotranspiration, soil moisture changes), model quality is related to
104 parsimony and data homogeneity. Here, we only rely on SST and rainfall data since
105 they are more accurately derived from remote sensing observations compared to
106 the other possible indicators (see, e.g., Reynolds et al., 2002, Huffman and Bolvin,
107 2012, Wang and Dickinson, 2012).

108 Time-variable maps of predictors (SST and rainfall data) and predictands
109 (TWS data) include large temporal and spatial correlations. This requires ap-
110 plication of a dimension reduction method before constructing the mathematical
111 relationship between predictors and predictands (e.g., Kaplan et al., 1997). This
112 considerably improves the skill of the forecasting approach (see e.g., Westra et al.,
113 2008). The statistical method of independent component analysis (ICA) was ap-
114 plied to extract individual modes of variability that are mutually independent and
115 successively explain the maximum amount of existing variance in the data (Fo-
116 rootan and Kusche, 2012, 2013). An optimum autoregressive model with exogenous
117 variables (ARX) (Ljung, 1987) was then used to relate independent components
118 (ICs) of predictands to ICs of predictors. In the end, the model allows a thor-
119 ough representation of complex processes in a highly efficient way as compared
120 to physical models. The combination of ICA/ARX modeling can be generalized
121 worldwide, with an adequate identification of likely forcing recalibration of the
122 model, with respect to the region of interest. Examples include the regions such
123 as North America and the Australian continent, which exhibit strong ocean-land-
124 atmosphere interactions (Douville et al., 2006, Forootan et al., 2012).

125 From a methodological point of view, we prefer the ICA algorithm for dimen-
126 sion reduction over, e.g., principal component analysis (PCA, Preisendorfer, 1988);
127 this view is rooted in the improved performance of ICA in extracting trends, an-
128 nual patterns, as well as slow dynamic patterns such as the El Niño-Southern
129 Oscillation (ENSO) from climate observations (e.g., Aires et al., 2002, Ilin et al.,
130 2005)). In a preliminary study, Forootan and Kusche (2012) and Forootan et al.
131 (2012) applied the ICA method to global and local GRACE-TWS time series, and
132 demonstrated its value in extracting climate related patterns. We also evaluated
133 the use of PCA in our proposed statistical TWS forecast (results are not shown
134 here), and found that ICA improves the extraction of teleconnections, e.g., ENSO
135 and the Indian Ocean Dipole (IOD) patterns, as well as the performance of the
136 prediction. A similar conclusion was reached, e.g., by Westra et al. (2007), who
137 assessed the performance of ICA and PCA for simulating hydrological time series.

138 Finally, we prefer the ARX model over the common canonical correlation anal-
139 ysis (CCA) approach (e.g., von Storch and Navara, 1999) for relating predictors
140 and predictands since ARX offers more flexibility to relate multiple parameters as
141 exemplified e.g., in Westra et al. (2008).

142 To implement our prediction approach, first, we begin by decomposing the
143 following data sets individually into statistically independent modes: (i) GRACE-
144 TWS changes over West Africa, to provide the dominant independent patterns of
145 total water storage (TWS) that are subsequently identified with the predictands
146 of the ARX process; (ii) SSTs over the Atlantic, Pacific, and Indian Ocean basins,
147 in order to extract ocean-atmospheric interactions and teleconnections; and (iii)
148 TRMM data over West Africa, for extracting the main patterns of rainfall over
149 the region. Then, the modes found by analyzing (ii) and (iii) are introduced as
150 predictors of (i) within the ARX process model, while using the first 72 months
151 of (i), (ii) and (iii) for the training step (statistical simulation). The fitted ARX
152 model, along with the independent modes of SST and rainfall (i.e. the predictors
153 of the ARX model) after the 72th month are then used to predict TWS after
154 the simulation period. The prediction is evaluated using those GRACE-derived
155 TWS anomalies that are available after the simulation period. Forecasting error
156 levels are also predicted using a Monte Carlo error estimation process. We should
157 mention here that to decompose water storage and rainfall data in (i) and (iii), we
158 introduced the West Africa region as a simple box (latitude between 0° to $25^\circ N$
159 and longitude between -20° to $10^\circ E$). The method, however, can be extended to
160 grids delineated by basin shape or basin-averaged time series.

161 This contribution is organized as follows; in Section 2, we briefly present the
162 data sets used in the study. The dimension reduction and the ARX forecasting
163 methods are introduced in Section 3, followed in Section 4 by a discussion of the
164 leading independent modes found in the total water storage (TWS), sea surface
165 temperature (SST) and rainfall data sets. In Section 5, we discuss the results of
166 ARX-TWS simulations and forecasts over West Africa. The study is concluded in
167 Section 6. The paper also contains two appendices. In Appendix A, the details of
168 GRACE-TWS estimations over West Africa are described, and in Appendix B, we
169 present the details of mathematical methods, used in this study, including ICA,
170 and the ARX model as well as their uncertainty estimations.

171 **2 Data**

172 **2.1 Total Water Storage from GRACE and WGHM**

173 The GRACE mission consists of two low-earth orbiting satellites in the same or-
174 bital plane at the current altitude of ~ 450 km and in an inclination of 89.5° . The
175 separation distance between the two satellites is measured precisely by a K-band
176 ranging system and the location of each satellite is determined by GPS receivers
177 on-board the spacecraft (Tapley et al., 2004). These data, after application of sev-
178 eral corrections, are then used by a number of analysis to generate time-variable
179 (usually monthly) Level-2 gravity field products (Flechtner, 2007). In this study,
180 we used monthly GRACE products from the German Research Centre (GFZ)
181 Potsdam (Flechtner, 2007) for computing TWS fields, covering August 2002 to
182 May 2011. We did not interpolate the missing data of January 2003, 2004, May

183 2003, and December 2008 in order to avoid creating artifacts. For comparison, we
184 also used monthly GRACE-ITG2010 products from Bonn University, Germany
185 (Mayer-Gürr et al., 2010), which are available for the period between September
186 2002 and August 2009, and are provided together with full variance-covariance
187 information. The covariance matrices were used to estimate the accuracy of the
188 GRACE-TWS grids. Total water storage from GRACE are also compared with
189 TWS output from the WGHM model (Döll et al., 2003), covering the years 2003
190 to 2010. WGHM represents the major hydrological components, such as soil mois-
191 ture, rainfall, snow accumulation, melting, evaporation, runoff, and the lateral
192 transport of water within river networks. For this study, we prefer WGHM over
193 using land surface models (LSM) since it also contains a groundwater simulation
194 model and, therefore, its vertically aggregated storage can be directly compared
195 to GRACE TWS. The details of data preparation are described in Appendix A.

196 2.2 SST

197 Monthly reconstructed global $1^\circ \times 1^\circ$ Reynolds sea surface temperature (SST)
198 data (Reynolds et al., 2002) were used over the period 2002 to 2012. The Reynolds
199 SST has been frequently used for climate studies, including some addressing African
200 rainfall variability in relation to SST (e.g., Mohino et al., 2011, Omondi et al.,
201 2012). Similar to Omondi et al. (2012), the SST data cover three major ocean
202 basins: we include an Atlantic Ocean box (-66° to 13° E and -20° to 31° N), a
203 Pacific Ocean box (159° to 275° E and -30° to 19° N) and an Indian Ocean box
204 (34° to 114° E and -50° to 1° N). Sea surface temperatures in these regions are
205 then extracted and analyzed through the ICA approach (Section 4). We found that
206 a slight difference in the size of the selected boxes would not change the results of
207 ICA significantly.

208 2.3 TRMM

209 Version 7 of TRMM-3B42 products (Huffman and Bolvin, 2012) covering 2002 to
210 2012 (<http://mirador.gsfc.nasa.gov/>) was used. The downloaded 3-hourly rainfall
211 rates have been converted to rainfall amount and aggregated to monthly basis.
212 TRMM was previously used e.g., by Nicholson et al. (2003) to study the patterns
213 of precipitation over West Africa. Huffman and Bolvin (2012) and Fleming and
214 Awange (2013) reported a significant improvement of version 7 over version 6,
215 likely as a result of including more microwave sounding and imagery records as
216 well as implementing better processing algorithms.

217 3 Methodology

218 3.1 Identifying Dominant Independent Patterns from Available Data

219 In order to keep the problem of identifying independent modes on a grid, in-
220 cluding the statistical relationships between them, numerically manageable, it is
221 mandatory to first apply a dimension reduction method before constructing the

222 mathematical relationship between predictors and predictands (e.g., Kaplan et al.,
 223 1997). This improves the prediction skills of the statistical approach, since the re-
 224 dundant information within the data sets, both predictors and predictands, will
 225 be reduced. Dimension reduction is implemented here by applying a 2-step inde-
 226 pendent component analysis (ICA) algorithm (Forootan and Kusche, 2012, 2013)
 227 to the TWS, rainfall, and SST data sets. Forootan and Kusche (2012) formulate
 228 two alternative ways of applying ICA, in which either temporally independent
 229 components or spatially independent components are constructed. The temporal
 230 ICA method, which we simply abbreviate here as ICA, is preferred in this study
 231 since it provides temporally independent components that allow the development
 232 of a prediction model that is univariate in the predictand (see Section 3.2).

233 Let us assume that GRACE-TWS anomalies (in mm), after removing the tem-
 234 poral mean, are stored in the matrix $\mathbf{X}_{TWS} = \mathbf{X}_{TWS}(s, t)$, where t is the time,
 235 and s stands for spatial coordinate (grid points). Applying ICA means that \mathbf{X}_{TWS}
 236 is decomposed into spatial and temporal components as

$$\mathbf{X}_{TWS} = \mathbf{Y}_j \mathbf{A}_j^T, \quad (1)$$

237 where the columns of \mathbf{Y}_j contain the j dominant unit-less temporally independent
 238 components (ICs) of TWS, and the columns of \mathbf{A}_j represent the corresponding
 239 spatial maps. Each temporal pattern (i.e. a column of \mathbf{Y}_j) along with the cor-
 240 responding spatial pattern (a column of \mathbf{A}_j) represent an independent mode of
 241 variability. Likewise, the temporally centered maps of rainfall over West Africa
 242 $\mathbf{X}_{Rainfall}$, and of SST over the major oceans \mathbf{X}_{SST} can separately be written as

$$\mathbf{X}_{SST \text{ or } Rainfall} = \mathbf{U}_{j'} \mathbf{B}_{j'}^T, \quad (2)$$

243 where $\mathbf{U}_{j'}$ stores the j' dominant unit-less temporally independent components of
 244 SST or rainfall, and the columns of $\mathbf{B}_{j'}$ contain the associated spatial maps. We
 245 used different indices j and j' in Eqs. (1) and (2) to emphasize that the number
 246 of retained modes from different data sets are not necessarily the same. Selecting
 247 a proper subset (j or j') is addressed in Appendix B.

248 In our analysis, we found the spatial patterns associated with independent
 249 modes of total water storage anomalies, i.e. the columns of \mathbf{A}_j (Eq. (1)) to be
 250 sufficiently stable. This means that, for instance, the spatial patterns (\mathbf{A}_j) derived
 251 from 10 years of TWS data do not differ significantly from those derived from 8
 252 or 12 years of data. Therefore, for building the forecasting model, we only link
 253 the temporal components (ICs) of the predictor data sets (all columns of $\mathbf{U}_{j'}$
 254 derived from SSTs and TRMM-rainfall) to individual ICs of the predictand (each
 255 column of \mathbf{Y}_j in Eq. (1)). Finally, we will use the \mathbf{A}_j derived from TWS in order
 256 to reconstruct the forecasting maps. Details of the ICA decomposition and the
 257 corresponding error estimation are addressed in Appendix B.

258 3.2 Prediction using an Autoregressive Model with Exogenous Variables (ARX)

259 An ARX process is governed by a system of linear equations, which describe the
 260 relationship between the current and previous values of the system output and the
 261 values of inputs. In our case, the ARX model is formulated as a multiple-input

262 (the independent modes or ICs of SST and rainfall all together) and single-output
 263 (each IC of TWS) model (Ljung, 1987):

$$y(t) + \sum_{i=1}^{n_a} a_i y(t-i) = \sum_{q=1}^m \sum_{l=1}^{n_b} b_{q,l} u_q(t-k_q-(l-1)) + \xi(t), \quad (3)$$

264 where y represents a particular mode of TWS, i.e. $y(t)$, $t = 1, \dots, n$, represent
 265 a column of \mathbf{Y}_j in Eq. (1). In Eq. (3), n_a is the order of the ARX model with
 266 respect to the predictand, $u_q(t)$, $q = 1, \dots, m$, and $t = 1, \dots, n$, are ICs of SSTs
 267 and rainfall from $\mathbf{U}_{j'}$ in Eq. (2), while m is the number of predictors. The order of
 268 the ARX model with respect to the predictors is n_b , and k_q denotes the number of
 269 time-steps before the q 'th input (predictor) affects the output y , i.e. the dead time
 270 of the system. Finally, ξ allows for a white-noise random input. The coefficients
 271 of the ARX models a_i , $i = 1, \dots, n_a$, and $b_{q,l}$, $q = 1, \dots, m$, and $l = 1, \dots, n_b$,
 272 have to be derived in the simulation step, using both predictand and predictors
 273 (Ljung, 1987). Once the coefficients are computed, in the forecasting step only
 274 the predictors (ICs of SST and rainfall) are used to estimate the values of TWS
 275 after the simulation period. Details of the computations and error propagation are
 276 addressed in Appendix B.

277 4 Dominant Independent Modes of TWS, SST, and Rainfall

278 When following the decomposition procedure as described in Section 3.1, we identify
 279 two independent, statistically significant, modes in GRACE GFZ-TWS (abbreviated as GFZ-TWS),
 280 four independent modes in SST changes over the Atlantic Ocean, three modes over the Pacific
 281 Ocean, and four modes over the Indian Ocean. For the rainfall changes, also four significant
 282 independent modes were obtained. Our approach for separating significant modes from the
 283 insignificant ones is also presented in Appendix B. Finally, Table 1 summarizes the variance
 284 percentage of the modes discussed so far.
 285

Table 1 List of the variance percentage that each of the independent mode in Section 4 represents. Independent modes of GRACE GFZ-TWS are shown in Fig. 1, a and b, those of the Atlantic, Pacific and Indian Ocean-SST are shown in Fig. 2. Fig. 3 contains the independent modes of TRMM-rainfall.

	First Independent Mode	Second Independent Mode	Third Independent Mode	Fourth Independent Mode
GRACE GFZ-TWS	62.4%	20.4%		
WGHM-TWS	60.4%	16.4%		
Atlantic Ocean-SST	46.4%	25.4%	11.7%	4.1%
Pacific Ocean-SST	55.6%	15.4%	14.6%	
Indian Ocean-SST	47.8%	15.4%	14.3%	11.1%
TRMM-rainfall	44.2%	12.3%	6.9%	6.4%

286 *Dominant Independent Modes Identified in Total Water Storage Variability*

287 The first and second independent modes the from TWS anomalies derived from
 288 GRACE (GFZ solutions) are shown in Fig. 1,a. The first dominant independent
 289 mode, which explains 62.4% of variance, represents the annual water variability
 290 over West Africa. Here a damping of the signal magnitude can be seen in the year

291 2005 (temporal IC1 of GRACE GFZ-TWS). From the spatial pattern of IC1, a
292 concentration of annual variability appears to be dominant over the tropic and
293 coastal regions. The second mode of GRACE-TWS contains inter-annual varia-
294 tions, along with periodic components of ~ 3 and 5 years period. Nicholson (2000)
295 found a similar period in rainfall variations over West Africa. The second inde-
296 pendent mode represents 20.4% of the GRACE-TWS variance, thus, the first two
297 leading modes in Fig. 1 represent more than 80% of the TWS variance over West
298 Africs. In fact, the dominating annual and inter-annual variability of TWS are
299 found well separated, and thus can be treated separately within the ARX simula-
300 tion and prediction steps. We attribute this behavior to the properties of the ICA
301 decomposition method.

302 The separate treatments of the two annual and inter-annual variability of wa-
303 ter storage components seems to be reasonable since they are likely due to differ-
304 ent physical influences from environment (here the indicators SST and rainfall).
305 Therefore, the mathematical relationship between TWS and its indicators must
306 be separately weighted (i.e. coefficients a_i , $i = 1, \dots, n_a$, and $b_{q,l}$, $q = 1, \dots, m$ of
307 IC1-GRACE and IC2-GRACE will be separately computed in Eq. 3). We would
308 like to mention here that the oscillations that exist in the extracted dominant
309 independent modes are not necessarily explained by a fundamental annual or
310 inter-annual cycle and its overtones. Therefore, for the decomposition and pre-
311 diction procedures, we chose not to reduce any such pre-defined oscillations (see
312 also Schmidt et al. 2008b).

313 For comparison, we then projected WGHM-TWS and ITG2010-TWS on to the
314 spatial patterns of Fig. 1,a, using Eq. (B2) (Appendix B). The results are shown
315 by the black and gray lines in Fig. 1,a. The temporal patterns indicate that the
316 annual TWS changes from WGHM (IC1 in Fig. 1,a) are comparable to those seen
317 by GRACE, whereas at the inter-annual time scale they are different (see IC2 in
318 Fig. 1,a). To confirm this finding, we also applied ICA (Eq. (1)) to the WGHM-
319 TWS data, individually, with the results shown in Fig. 1,b. The first independent
320 mode of WGHM-TWS (60.4% of variance) is comparable to that of GRACE-TWS,
321 while the second mode of WGHM-TWS (spatial and temporal pattern of IC2-
322 WGHM) that accounts for 16.4% of variance is found quite different from those
323 of GRACE-TWS (both GFZ and ITG2010). This finding shows that WGHM-
324 TWS and GRACE-TWS are not consistent at inter-annual time scale; compare
325 Fig. 1,a with Fig. 1,b. We hypothesize that the difference could be attributed to
326 the possible miss-modeling of surface water storage or water withdrawals over the
327 region. Further research will be needed to address the exact cause of differences,
328 but this is outside the scope of the current study.

329 *Dominant Independent Modes of Sea Surface Temperature and Rainfall Data*

330 Applying the ICA approach (Eq. (2)) to SST changes over the three ocean boxes
331 shows that their first two independent modes are related to the annual variability
332 of SST (IC1 and IC2 in Fig. 2,a,b, and c). Over the Atlantic, for instance, IC1
333 and IC2 are related to the annual dipole structure, which also correlate very much
334 with IC1 of GFZ-TWS. The same damping of the annual amplitude in the year
335 2005 is seen for IC2-Atlantic SST, similar as with IC1 of GFZ-TWS. Our result
336 confirms that the recent annual variability of total water storage over West Africa
337 is highly correlated with the Atlantic ocean-atmospheric interactions, reflected in

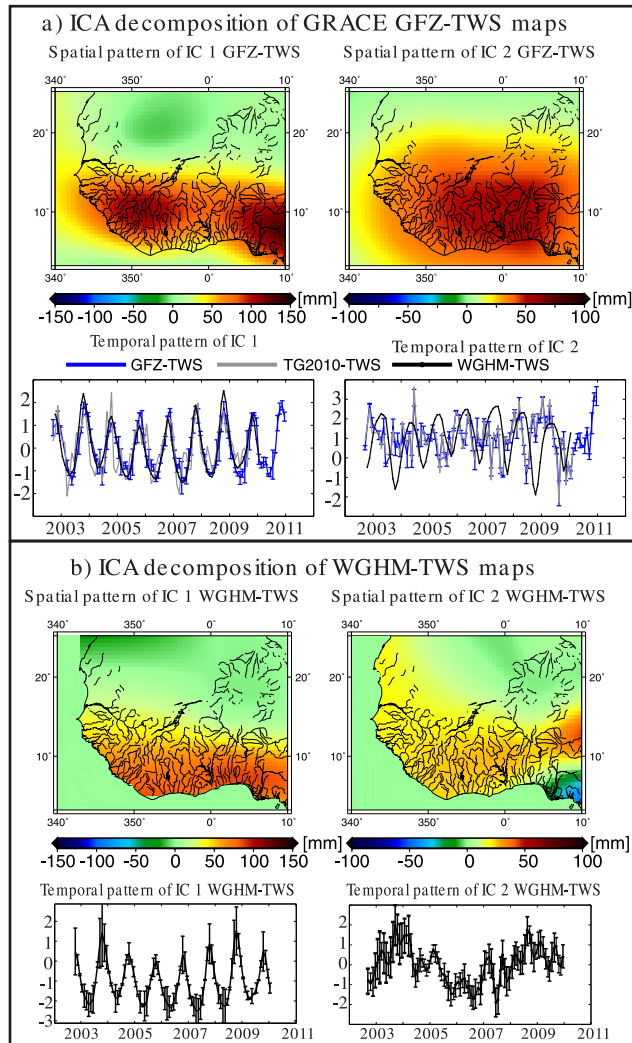


Fig. 1 Overview of the ICA decomposition of TWS changes over West Africa (counted as predictands). a) ICA decomposition of GRACE GFZ-TWS data (GFZ-TWS). For comparisons, WGHM-TWS and ITG2010-TWS changes are projected on the spatial patterns of IC1 and IC2, using Eq. B2 in Appendix B. The results are presented along with temporal ICs of GFZ-TWS. b) ICA decomposition of WGHM-TWS maps. The variance fraction of each independent mode is presented in Table 1. Uncertainties are shown by error-bars around temporal components. Details of uncertainty computations can be found in Appendix B.

338 the SST data (see similar findings in e.g., Mohino et al., 2011). For the variance
 339 percentages that each mode represents, we refer to Table 1.

340 We find that the third mode of SST changes over the Atlantic and Indian
 341 Ocean boxes represents semi-annual variability, while IC3-Pacific SST represents
 342 the ENSO pattern; we compared IC3-Pacific SST with the monthly ENSO pat-
 343 tern (shown by the Southern Oscillation Index (SOI)) provided by the Australian

344 Bureau of Meteorology (<http://www.bom.gov.au/climate/enso/>). A high correla-
345 tion of 0.84 was obtained, suggesting that the pattern is physically meaningful
346 (IC3 in Fig. 2,b). We also found a significant correlation of 0.68 between IC2 of
347 GRACE-TWS (Fig. 1,a) and SOI, revealing a relationship between total water
348 storage variability over West Africa and ENSO.

349 IC4-Atlantic SST represents a complicated pattern, which we do not attempt
350 to interpret here. IC4-Indian SST (Fig. 2,c) follows the Indian Ocean Dipole (IOD)
351 pattern (see e.g., Saji et al., 1999). Comparing our results to the IOD index derived
352 from the Japan Agency for Marine-Earth Science and Technology (JAMSTEC,
353 <http://www.jamstec.go.jp/frcgc/research/>

354 [d1/iod/HTML/Dipole%20Mode%20Index.html](http://www.jamstec.go.jp/frcgc/research/d1/iod/HTML/Dipole%20Mode%20Index.html)) represents a significant corre-
355 lation of 0.73. This shows that ICA extracts teleconnection patterns from SST
356 data fairly well.

357 Four independent modes were extracted from TRMM-rainfall data, from which
358 IC1-TRMM and IC2-TRMM relate to the annual rainfall variability with three
359 months phase differences (Fig. 3). In 2005, a damping of the signal magnitude can
360 be seen in IC2-TRMM, but it is less pronounced compared to that of IC2-Atlantic
361 SST. This might be due to the fact that IC2-TRMM represents a local impact,
362 compared to the large-scale interaction that IC2-Atlantic SST represents. IC3-
363 TRMM and IC4-TRMM apparently represent the semi-annual rainfall variations.
364 We found a lag of two months between the ICs of rainfall and those of TWS.

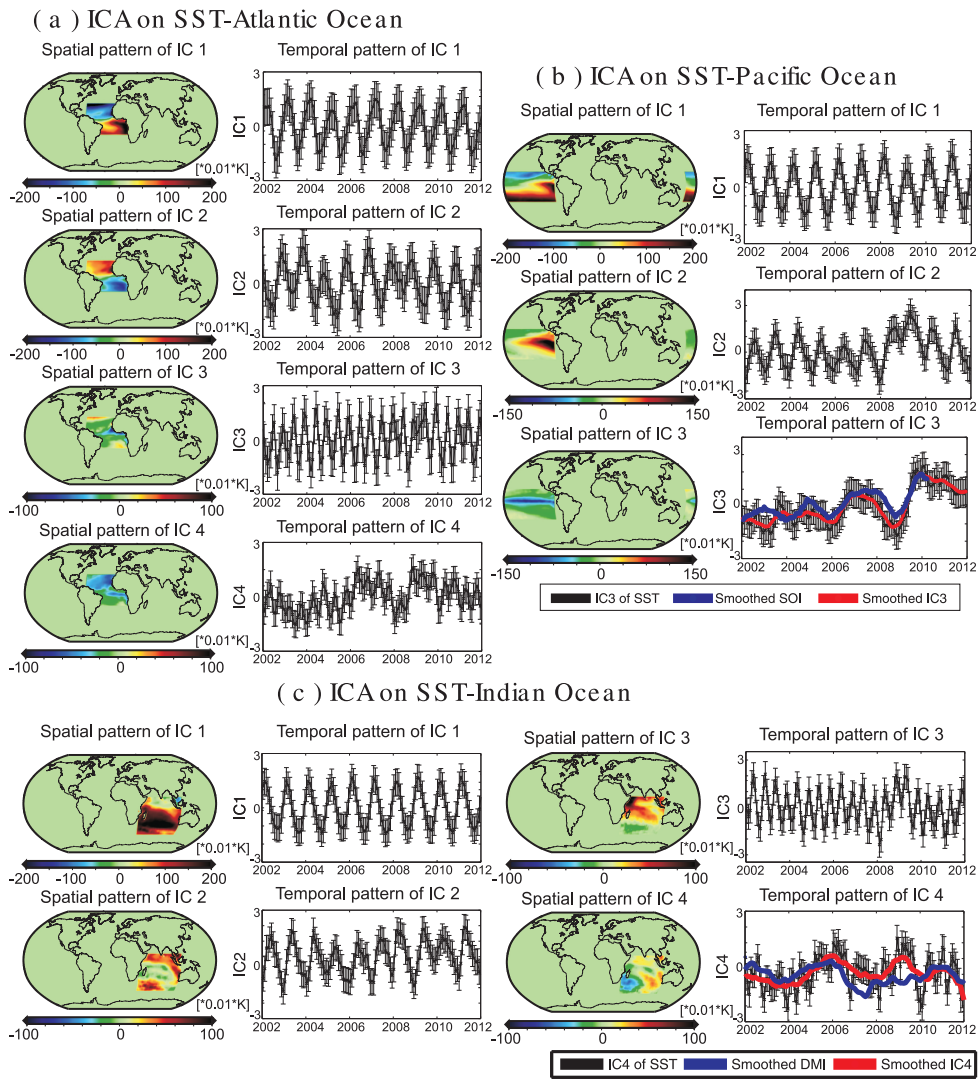
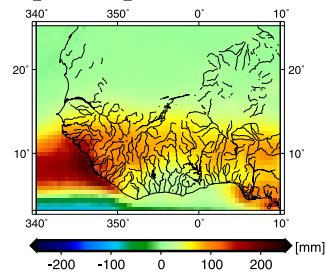
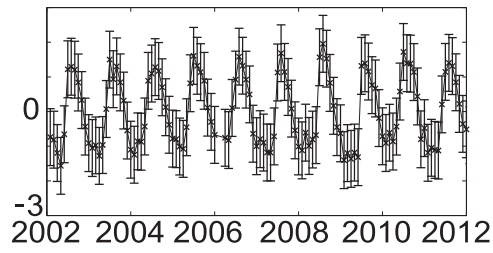


Fig. 2 Overview of ICA decomposition applied to the SST changes over (a) the Atlantic, (b) Pacific, and (c) Indian Oceans. The variance fraction of each independent mode is presented in Table 1. Uncertainties are shown by error-bars around temporal components. The smoothed temporal patterns in (a) and (b) are derived by applying a 12-month moving average filter.

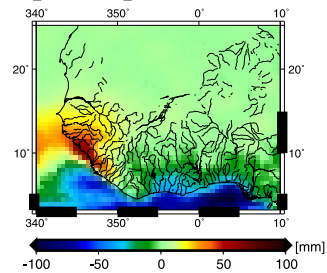
Spatial pattern of IC 1



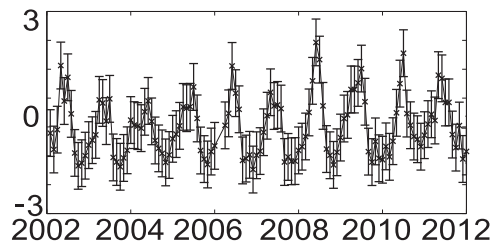
Temporal pattern of IC 1



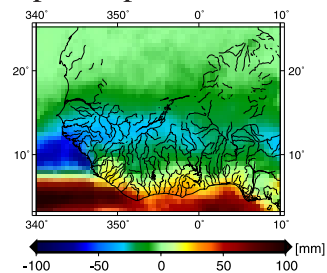
Spatial pattern of IC 2



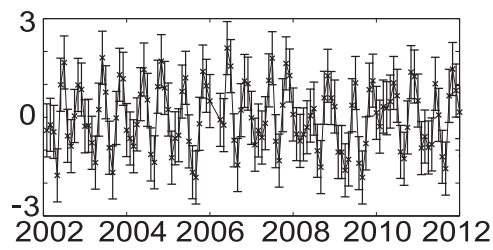
Temporal pattern of IC 2



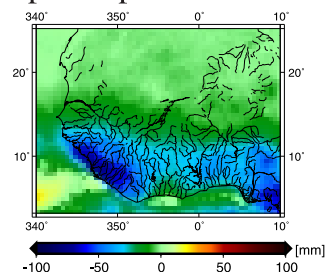
Spatial pattern of IC 3



Temporal pattern of IC 3



Spatial pattern of IC 4



Temporal pattern of IC 4

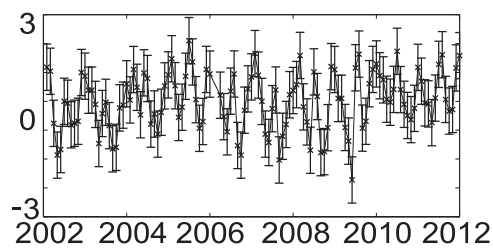


Fig. 3 Overview of ICA decomposition applied on rainfall changes over West Africa. The variance fraction of each independent mode is presented in Table 1. Uncertainties are shown by error-bars around temporal components.

365 **5 Predicting Total Water Storage with an Autoregressive Model**

366 *Training Step*

367 To compute the best-fitting ARX model, we have inserted the first 72 months
 368 of each mode of GRACE GFZ-TWS (IC1 and IC2 in Fig. 1,a) and the first 72
 369 months of all temporal modes of SST and rainfall (ICs of Figs. 2 and 3) in Eq.
 370 (3). Before performing the training step of the ARX model, the data for January
 371 2003, 2004, May 2003 and December 2008 were excluded from the input time series
 372 (ICs of SSTs and rainfall) to synchronize them with the GFZ-TWS time series.
 373 Then, we had to choose optimum n_a and n_b ; these were found experimentally by
 374 varying them between one to three. The time delay k_q was searched for between
 375 zero and three months. This was then followed by running the ARX simulation
 376 step (Eq. (3)). We did not consider higher orders for n_a and n_b since we would
 377 like to keep the forecasting model as simple as possible (e.g., Westra et al., 2008).
 378 For k_q , previous studies (e.g., Ahmed et al., 2011) found a delay of up to three
 379 months between SST-rainfall and TWS changes. The required coefficients for each
 380 ARX model $\hat{\Theta}$ were computed using Eq. (B5) in Appendix B.

381 Our numerically simulated results for both IC1 and IC2 of GFZ-TWS suggest
 382 that an ARX model with $n_a=1$ and $n_b=3$ provides the best fit with the residuals
 383 passing the normality test. The RMS of differences between the simulated TWS
 384 values from the ARX process and the ICs of GFZ-TWS (Eq. (B6) in Appendix
 385 B) was used as the fit criterion. Two sets of k_q corresponding to the simulations
 386 of the IC1 and IC2 of GFZ-TWS were found and are presented in Table 2. Our
 387 simulation results indicate that the ARX models provide a fit of 93% and 83%
 388 for simulating the two dominant components of GFZ-TWS (IC1 and IC2 in Fig.
 389 1,a), respectively. The simulation fit of ARX corresponding to IC2 of GFZ-TWS
 390 is, however, lower than that of IC1 since its temporal pattern appears much more
 391 complicated than the annual pattern in IC1. Therefore, it might not have been
 392 fully captured by the predictors (see Fig. 4).

Table 2 Time delays k_q derived from simulation of IC1-GRACE GFZ-TWS and IC2-GRACE GFZ-TWS. The values are in month and denote the number of time-steps before each predictor (ICs of SSTs and ICs of TRMM-rainfall respectively in Figs. 2 and 3) affect the output (each individual IC of GRACE GFZ-TWS in Fig. 1, a).

	IC1 SST Atlantic Ocean	IC2 SST Atlantic Ocean	IC3 SST Atlantic Ocean	IC4 SST Atlantic Ocean	IC1 SST Pacific Ocean	IC2 SST Pacific Ocean	IC3 SST Pacific Ocean	IC1 SST Indian Ocean	IC2 SST Indian Ocean	IC3 SST Indian Ocean	IC4 SST Indian Ocean	IC1 TRMM West Africa	IC2 TRMM West Africa	IC3 TRMM West Africa	IC4 TRMM West Africa
k_q related to IC1 of GFZ-TWS	1	0	2	1	0	3	1	1	0	1	0	0	3	3	1
k_q related to IC2 of GFZ-TWS	1	0	1	1	0	0	1	1	0	1	0	1	3	1	3

393 To assess the sensitivity of the ARX models (Eq. (3)) with respect to each
 394 input, first, for each IC of GFZ-TWS, each IC of Figs. 2 and 3 was individually
 395 inserted in Eq. (3) and the ARX model evaluated. For each IC of GFZ-TWS,
 396 therefore, an ensemble of 15 ARX-modeled TWS outputs was generated, and the
 397 correlations of these outputs and the ICs of GFZ-TWS were then computed. From
 398 the 15 ARX-generated TWS, those that represented the largest correlations with
 399 their corresponding IC of GFZ-TWS were likely to have the most influence on the
 400 prediction. Our results show that the ARX-outputs generated by IC1, IC2-Atlantic

401 SST, and IC1-rainfall had the largest influences on the ARX model of IC1 GFZ-
402 TWS. The prediction of IC2 GFZ-TWS was found to be sensitive to IC3-Pacific
403 SST, IC3-Atlantic SST, and IC3-rainfall. The most sensitive indicators and the
404 correlations of the associated outputs with the ICs of GFZ-TWS are presented
405 in Table 3. One might use these results for model reduction of the original ARX
406 process (see e.g., Westra et al., 2008), however, such a reduction was not applied
407 in this study since (i) the fit derived from each of the 15 model run was smaller
408 than that of original ARX run, and (ii) the ARX models apparently possessed
409 sufficient degree of freedom to be computed based on the current indicators.

Table 3 List of the most sensitive indicators derived from the ARX models for each input and the computed correlation of the output with IC1 and IC2 of GRACE GFZ-TWS. Correlations are derived at 95% level of confidence.

Rank:	1	2	3
Model run by:	IC1 SST Atlantic Ocean	IC2 SST Atlantic Ocean	IC1 TRMM-rainfall West Africa
Correlation with IC1 of GFZ-TWS	0.81	0.61	0.52
Model run by:	IC3 SST Pacific Ocean (ENSO)	IC3 SST Atlantic Ocean	IC3 TRMM-rainfall West Africa
Correlation with IC2 of GFZ-TWS	0.59	0.46	0.42

410 *ARX Forecasting Step and Validation*

411 Having simulated the ARX model parameters for the two dominant independent
412 modes of GFZ-TWS ($\hat{\Theta}$ is known from Eq. (B5), within the training step), we used
413 the indicator time series, i.e. all ICs shown in Figs. 2 and 3 after the 72-months
414 training period alone to predict ICs of GRACE GFZ-TWS changes for the years
415 2010 and 2011. The predictions were derived from Eq. (B8), and their uncertainties
416 were evaluated using the Monte Carlo approach described in Appendix B. Training
417 and forecast results are shown in Fig. 4a,b. Our prediction approach, therefore,
418 uses only the process structure described in Section 3.2 and the determined lag
419 relation between the predictors and ICs of GFZ-TWS changes (i.e. Table 2). The
420 fit of the forecast for the first leading mode of total water storage, when compared
421 to the observed GFZ-TWS values, after one year was found 79%, while after two
422 years this reduced to 62%. As Fig. 4a also shows, after two years, the standard
423 deviation of the propagated uncertainty is quite large. This suggests that the
424 proposed approach is more or less reliable for predictions of up to two years. Fig.
425 4b shows that the fit of the forecast for the second leading independent pattern of
426 total water storage after one year was reduced to 67%. After two years, a fit of 57%
427 was found. Comparing projected values of WGHM-TWS (black lines in Fig. 1a)
428 with the ICs of GFZ-TWS, during the first year of forecast, we found a fit of 78%

Table 4 List of the computed fit values (Eq. B6) derived from comparing the ARX-TWS outputs with the IC1 and IC2 of GRACE GFZ-TWS. We also compared the projected values of WGHM-TWS in Fig. 1 with the IC1 and IC2 of GRACE GFZ-TWS. The values indicate that the ARX outputs are closer to that of GRACE GFZ-TWS.

	Simulation period (72 months)	First year of the forecast	Second year of the forecast
Fit values of the ARX model with respect to IC1 of GFZ-TWS:	93%	79%	62%
Fit values of the ARX model with respect to IC2 of GFZ-TWS:	83%	67%	57%
Fit values of the WGHM model with respect to IC1 of GFZ-TWS:	91%	78%	43%
Fit values of the WGHM model with respect to IC2 of GFZ-TWS:	54%	53%	31%

429 for the annual and a moderate fit of 53% for the inter-annual pattern. This result
 430 indicates that the TWS prediction from the proposed statistical method is indeed
 431 closer to the observed GFZ-TWS changes over West Africa, when compared to
 432 hydrological modeling. See the fit values in Table 4.

433 Comparing the ARX-derived TWS predictions with the ICs of GFZ-TWS, dur-
 434 ing the forecast period, we found no apparent deviations between TWS time series
 435 (see Fig. 4a,b), thus, the reported fit values are significant. For the inter-annual
 436 time-scale, however, specific care should be taken since the simulation and pre-
 437 diction of the ARX-TWS method is very much sensitive to the temporal patterns
 438 of the input parameters. When the ICs of SSTs or rainfall are not well defined,
 439 the inter-annual forecast of ARX-TWS might perform poorly or be biased. This
 440 has been tested by replacing the ICs of SSTs and TRMM-rainfall with temporal
 441 components derived e.g., from the principal component analysis (PCA) decom-
 442 position for running the ARX predictions (results are not shown). A bias was found
 443 in the prediction of IC2 GFZ-TWS, which was most likely due to the fact that the
 444 PCA-derived indicators (PCs of SST and rainfall) do not reflect the inter-annual
 445 TWS changes sufficiently.

446 In order to assess the robustness of the performed forecast with respect to the
 447 training period, we performed a backward simulation and forecast, i.e. the last
 448 72 months of both indicators (ICs of SSTs and TRMM-rainfall) and predictands
 449 (individual ICs of GFZ-TWS) were used in the simulation step to predict the first
 450 two years of GFZ-TWS. The results, summarized in Fig. 5, show a fit similar to
 451 the forward forecast in Table 4. Therefore, even though the training step was quite
 452 short, no temporally variable bias was found in both forward and backward predic-
 453 tions. This confirms the robust performance of the proposed ICA-ARX approach,
 454 at least, with respect to the performed tests.

455 Inserting the time series of the prediction and the spatial components of Fig.
 456 1,a in Eq. (1), one may reconstruct the TWS maps for the period when the ARX
 457 model and their inputs are available. In this case, our prediction values provide \mathbf{Y}
 458 and the spatial maps of Fig 1,a provide \mathbf{A} in Eq. (1). Fig. 6 compares the original
 459 GRACE GFZ-TWS values of the year 2010, after removing the temporal mean of
 460 2003 to 2011 and the contribution of Lake Volta (as discussed in Section 3 and
 461 Appendix A), with the values of the ARX-TWS forecast. The predictions fit quite
 462 well to GFZ-TWS fields. Fig. 6,c shows the difference between GFZ-TWS and the
 463 predicted ARX-TWS. The patterns of the differences are similar to the striping

464 noise of GRACE solutions (Kusche, 2007). Our results, therefore, support the idea
 465 of using the presented statistical approach to forecast TWS changes over West
 466 Africa.

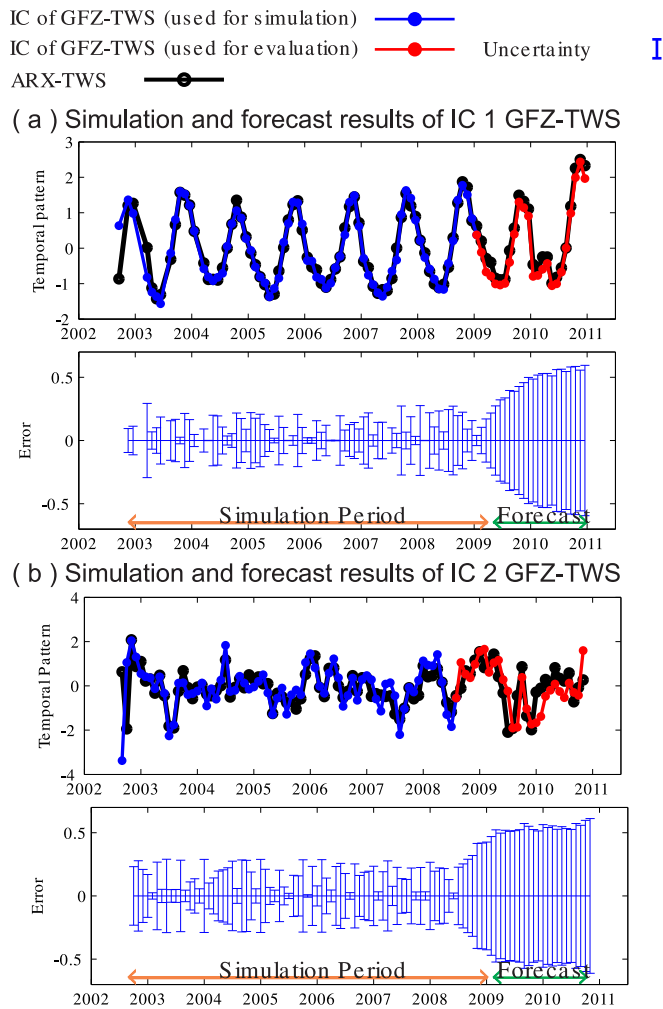
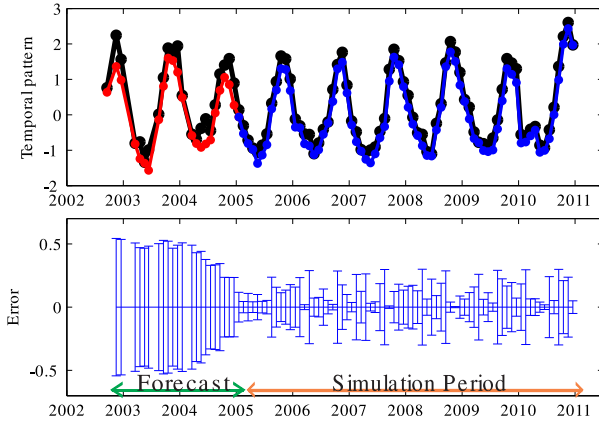


Fig. 4 Results of simulations and forecasts of IC1 and IC2 of GRACE GFZ-TWS (Fig. 1,a), using the ARX models (shown by black-lines). Fig. 4a(top) represents the results for IC1 of GRACE GFZ-TWS while assuming the ICs of Figs. 2 and 3 as indicators. Fig. 4a(bottom) shows the uncertainty of the forecast on top. Fig. 4b(top) represents the same results as (a) but corresponding to IC2 of GRACE GFZ-TWS. Fig. 4b(bottom) indicates the uncertainty of the forecast on top. For simulation, the first 72 months of TWS are used (shown in blue). TWS values after the 72th month are then used for evaluating the forecasts (shown in red). Reconstructing the forecast for the year 2010, and its comparison with the original GRACE GFZ-TWS fields are presented in Fig. 6.

IC of GFZ-TWS (used for simulation) —●—
 IC of GFZ-TWS (used for evaluation) —●— Uncertainty I
 ARX-TWS —●—

(a) Simulation and forecast results of IC 1 GFZ-TWS



(b) Simulation and forecast results of IC 2 GFZ-TWS

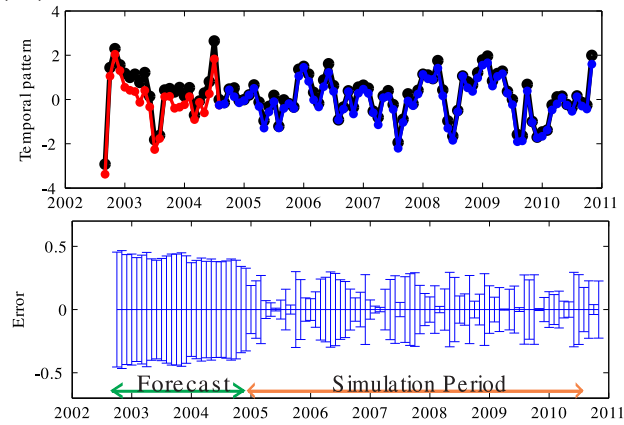


Fig. 5 Backward simulations and forecasts of IC1 and IC2 of GRACE GFZ-TWS (Fig. 1,a), using the ARX models (shown by black-lines). The results are similar to those of Fig. 4, however here, the last 72 months of both indicators (ICs of SSTs and TRMM-rainfall) and predictands (individual ICs of GRACE GFZ-TWS) are used in the simulations and the first two years of IC1 and IC2 of GRACE GFZ-TWS predicted. Fig. 5a(top) represents the results for IC1 of GRACE GFZ-TWS. Fig. 5a(bottom) shows uncertainty of the forecast on top. Fig. 5b(top) represents the same results as (a) but corresponding to IC2 of GRACE GFZ-TWS. Fig. 5b(bottom) indicates the uncertainty of the forecast on top.

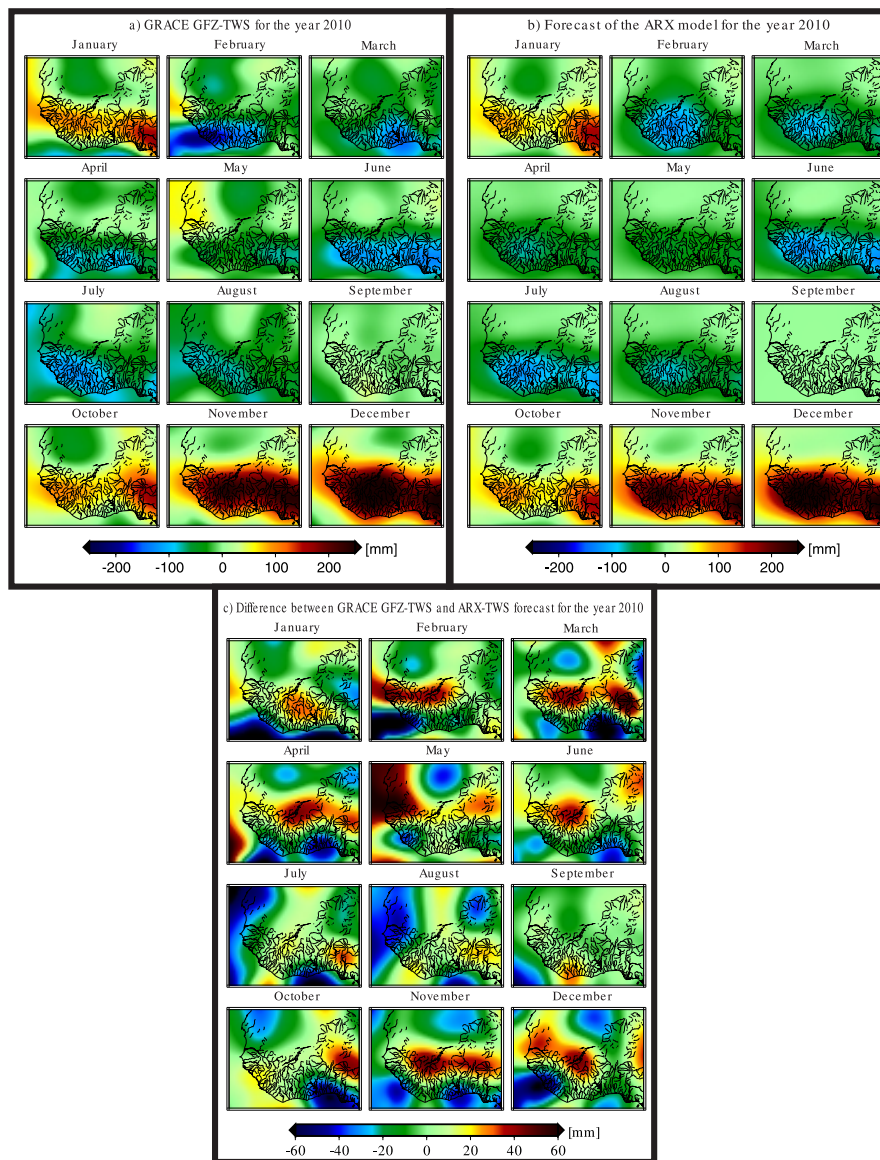


Fig. 6 Overview of TWS maps for the year 2010 over West Africa, without the signal of Volta, and after removing the temporal mean of 2003 to 2011. (a) TWS maps derived from GRACE (GFZ RL04 data), (b) TWS maps derived from the statistical forecast (the ARX models and ICA results), and (c) the differences between (a) and (b).

467 6 Conclusions and Outlooks

468 This study suggests and investigates a new statistical multivariate seasonal fore-
469 casting approach for total water storage (TWS), which uses sea surface tempera-
470 ture and rainfall data alone to estimate TWS changes over West Africa. The pro-
471 posed ICA/ARX approach does not directly simulate the complex physical process
472 of ocean-land-atmosphere, but instead, it statistically learns the relationships be-
473 tween main known physical processes of the region (such as teleconnections and
474 the soil-precipitation feedback) and uses it to predict TWS (the parameter of in-
475 terest). The successful implementation of the proposed ICA/ARX approach relies
476 on the proper selection of TWS indicators and avoiding over-parametrization of
477 the model, data homogeneity and a learning phase that contains a thorough range
478 of processes and impacts. Therefore, the dependence of the statistical model on the
479 climate characteristics of the calibration period is often referred as a lack of model
480 robustness. To investigate this issue, we performed a numerical validation, which
481 showed that the seasonal forecast of TWS is close to TWS that is actually mea-
482 sured by GRACE, see Table 4. Both forward and backward predictions indicate
483 that the proposed approach provides relatively stable large-scale seasonal TWS
484 forecast over West Africa. We also carried out an extensive uncertainty analysis
485 and were able to show that the predictability skills of the model is stable. However,
486 due to the estimated uncertainties, the results might not be significant after about
487 one year of forecast. We would like to mention here that the proposed method
488 is only able to provide predictions of total water storage, therefore, hydrological
489 modeling would still be required to partition TWS into different compartments.
490 Since the prediction method relies on the relationships between SST and rainfall as
491 indicators of TWS, we expect that the ICA/ARX method, with its current param-
492 eterization, is most appropriate to be used over those regions that exhibit strong
493 interactions between ocean-atmosphere and land water storage changes, which is
494 the case over West Africa.

495 Since the proposed method is trained on GRACE products, it provides rela-
496 tively coarse resolution TWS maps. The approach also assumes that the spatial
497 pattern of TWS changes remains stationary within the two years of the forecast.
498 Before application, one should therefore analyze whether this assumption is ful-
499 filled for different time frames. This can be achieved by applying the ICA technique
500 to TWS time series of different length, and evaluating whether the dominant spa-
501 tial patterns appear indeed invariant. Another issue is that the training of the
502 ARX model was performed based on six years of the data. Since SST and rain-
503 fall are available for a longer period (e.g., for TRMM, since 1998), one could use
504 TWS outputs of models for the time before 2002.8 and extend the training period.
505 Addressing the impact of such extension in terms of the quality of the ARX coeffi-
506 cients and the consistency of the model-derived TWS with GRACE-TWS requires
507 further research.

508 Our numerical results lead us to the hope that the presented statistical method
509 could be helpful for filling the current gaps of the GRACE products (once every
510 162 days, with one or two months of data is missing) and a possible gap period
511 between GRACE and its successor mission GRACE-FO at least for certain regions
512 such as West Africa. Another application of the presented approach could be the
513 generation of near-real time GRACE forecasts. Product latency time of GRACE
514 fields is currently two to three months, while using the suggested approach, one

515 could be able to forecast GRACE total water storage maps immediately as soon
516 as rainfall and sea surface temperature data become available. Such near-real time
517 predictions could be used for various drought/flood monitoring applications. Gen-
518 erating total water storage predictions, close to GRACE products, would also
519 be possible by calibrating and/or assimilating GRACE products in hydrological
520 models. Models improved in this way could then be used to simulate total water
521 storage. Examples of such implementations can be found in studies, e.g., Zaitchik
522 et al. (2008), Werth et al. (2009b), Houborg et al. (2012), and Xie et al. (2012).
523 The computational load of such approaches is however much more heavier than
524 with the proposed statistical ICA/ARX approach.

525 **Acknowledgement**

526 The authors would like to thank M.J. Rycroft (EiC) and anonymous reviewers for
527 their useful comments, which considerably improved this paper. We also thank S.
528 Nahmani (Laboratoire de Recherche en Géodésie, France) for his detailed com-
529 ments on the earlier version of this study. We are grateful for the GRACE, WGHM,
530 TRMM, and SST data, as well as climate indices used in this study. E. Forootan
531 and J. Kusche are grateful for the supports by the German Research Foundation
532 (DFG), under the project DFG BAYES-G. The Ohio State University compo-
533 nent of the research is supported by the NASA's Advanced Concepts in Space
534 Geodesy Program (Grant No. NNX12AK28G), and by the Chinese Academy of
535 Sciences/SAFEA International Partnership Program for Creative Research Teams
536 (Grant No. KZZD-EW-TZ-05). The authors are grateful for the data used in this
537 study. This is a TIGeR Publication no. xxx

- 539 Ahmed, M., Sultan, M., Wahr, J., Yan, E., Milewski, A., Sauck, W., Becker, R., & Welton,
540 B. (2011). Integration of GRACE (Gravity Recovery and Climate Experiment) data with
541 traditional data sets for a better understanding of the time-dependent water partitioning
542 in African watersheds. *Journal of Geology*, 41 (1), doi:10.1130/G31812.1.
- 543 Ali, A., & Lebel, T. (2009). The Sahelian standardized rainfall index revisited, *Int. J.*
544 *Climatol.*, 1714(December 2008), 1705-1714, doi:10.1002/joc.
- 545 Boone, A., Decharme, B., Guichard, F., de Rosnay, P., Balsamo, G., Beljaars, A., Chopin,
546 F., Orgeval, T., Polcher, J., Delire, C., Ducharne, A., Gascoin, S., Grippa, M., Jarlan,
547 L., Kergoat, L., Mougou, E., Gusev, Y., Nasonova, O., Harris, P., Taylor, C., Norgaard,
548 A., Sandholt, I., Ottlé, C., Pocard-Leclercq, I., Saux-Picart, S., & Xue, Y. (2009). The
549 AMMA Land Surface Model Inter-comparison Project (ALMIP), *Bull. Am. Meteorol. Soc.*,
550 90(12), 1865-1880, doi:10.1175/2009BAMS2786.1.
- 551 Chen, J.L., Wilson, C. R., Tapley, B.D., Longuevergne, L., Yang, Z.L., & Scanlon, B.R.
552 (2010). Recent La Plata basin drought conditions observed by satellite gravimetry, *J.*
553 *Geophys. Res.*, 115(D22), 1-12, doi: 10.1029 /2010JD014689.
- 554 Crétaux, J.-F., Jelinski, W., Calmant, S., Kouraev, A., Vuglinski, V., Bergé Nguyen,
555 M., Gennero, M.-C., Nino, F., Abarca Del Rio, F., Cazenave, A., & Maisongrande, P.
556 (2011). SOLS: a lake database to monitor in near real time water level and storage variations
557 from remote sensing data. *J. Adv. Space Res.*, 14971507, [http://dx.doi.org/10.1016/
558 j.asr.2011.01.004](http://dx.doi.org/10.1016/j.asr.2011.01.004).
- 559 Diatta, S., & Fink, A.H. (2014). Statistical relationship between remote climate indices and
560 West African monsoon variability. *Int. J. Climatol.* (2014), in-press, doi:10.1002/joc.3912.
- 561 Döll, P., Kaspar, F., & Lehner, B. (2003). A global hydrological model for deriving water
562 availability indicators: model tuning and validation. *Journal of Hydrology* 270 (1-2), 105-
563 134, doi:10.1016/S00221694(02)002834.
- 564 Douville, H., Conil, S., Tyteca, S. and Voltaire, a. (2006). Soil moisture memory and
565 West African monsoon predictability: artifact or reality?, *Clim. Dyn.*, 28(7-8), 723-742,
566 doi:10.1007/s00382-006-0207-8.
- 567 Efron, B. (1979). Bootstrap methods: Another look at the jackknife. *Ann. Statist.* 7, 1-26.
- 568 Eicker, A., Schumacher, M., Kusche, J., Döll, P., & Müller Schmied, H. (2014). Calibration/
569 data assimilation approach for integrating GRACE data into the WaterGAP Global
570 Hydrology Model (WGHM) using an ensemble Kalman filter. *Surveys in Geophysics*, submitted.
- 571
- 572 Flechtner, F. (2007). GFZ Level-2 processing standards document for level-2 product re-
573 lease 0004. GRACE 327-743, Rev. 1.0.
- 574 Fleming, K., & Awange, J.L. (2013). Comparing the version 7 TRMM 3B43 monthly
575 precipitation product with the TRMM 3B43 version 6/6A and BoM datasets for Australia.
576 *Australian Meteorological and Oceanographic Journal* (in press).
- 577 Forootan, E., Didova, O., Schumacher, M., Kusche, J., & Elsaka, B. (2014). Comparisons
578 of atmospheric mass variations derived from ECMWF reanalysis and operational fields,
579 over 2003 to 2011. *Journal of Geodesy*, 88 (5), 503-514, doi: 10.1007/s00190-014-0696-x.
- 580 Forootan, E., Didova, O., Kusche, J., & Löcher, A. (2013). Comparisons of atmospheric
581 data and reduction methods for the analysis of satellite gravimetry observations, *J. Geophys.*
582 *Res. Solid Earth*, 118, doi:10.1002/jgrb.50160.
- 583 Forootan, E., Awange, J., Kusche, J., Heck, B., & Eicker, A. (2012). Independent patterns
584 of water mass anomalies over Australia from satellite data and models. *Journal of Remote*
585 *Sensing of Environment*, 124, 427-443, doi:10.1016/j.rse.2012.05.023.
- 586 Forootan, E., & Kusche, J. (2013). Separation of deterministic signals, using independent
587 component analysis (ICA). *Stud. Geophys. Geod.* 57, 17-26, doi:10.1007/s11200-012-0718-
588 1.
- 589 Forootan, E., & Kusche, J. (2012). Separation of global time-variable gravity signals into
590 maximally independent components. *Journal of Geodesy*, 86 (7), 477-497, doi:10.1007/s00190-
591 011-0532-5.
- 592 Giannini, A., Saravanan, R., & Chang, P. (2003). Oceanic forcing of Sahel rainfall on
593 interannual to interdecadal time scales, *Science*, 302, 10271030.
- 594 Giannini, A., Biasutti, M., Held, I.M., & Sobel, A.H. (2008). A global perspective on
595 African climate. *Climatic Change* 90, 359-383, doi:10.1007/ s10584-008-9396-y.

596 Grippa, M., Kergoat, L., Frappart, F., Araud, Q., Boone, A., de Rosnay, P., Lemoine,
597 J.-M., Gascoin, S., Balsamo, G., Oettle, C., Decharme, B., Saux-Picart, S., & Ramillien,
598 G. (2011). Land water storage variability over West Africa estimated by Gravity Recovery
599 and Climate Experiment (GRACE) and land surface models. *Water Resources Research*
600 47, W05549, doi:10.1029/2009WR008856.

601 Güntner, A., Stuck, J., Döll, P., Schulze, K., Merz, B. (2007). A global analysis of tempo-
602 ral and spatial variations in continental water storage. *Water Resources Research* 43,
603 (W05416), doi:10.1029/2006WR005247.

604 Hansen, J.W., Mason, S.J., Sun, L. & Tall, A. (2011). Review of seasonal climate forecast-
605 ing for agriculture in sub-Saharan Africa, *Expl Agric.* 47 (2), pp. 205-240,
606 : <http://dx.doi.org/10.1017/S0014479710000876>.

607 Heim, R.R. (2002). A review of twentieth-century drought indices used in the United
608 States. *Bull. Amer. Meteor. Soc.*, 83, 1149-1165.

609 Houborg, R., Rodell, M., Li, B., Reichle, R. & Zaitchik, B.F. (2012). Drought indicators
610 based on model-assimilated Gravity Recovery and Climate Experiment (GRACE) terres-
611 trial water storage observations, *Water Resour. Res.*, 48, doi:10.1029/2011WR011291.

612 Huffman, G., & Bolvin, D. (2012). TRMM and other data precipitation data set documen-
613 tation. Mesoscale Atmospheric Processes Laboratory, NASA Goddard Space Flight Center
614 and Science Systems and Applications, Inc.

615 Ilin, A., Valpola, H., & Oja, E. (2005). Semiblind source separation of climate data detects
616 El Niño as the component with the highest interannual variability. In: *Proceedings of*
617 *the International Joint Conference on Neural Networks (IJCNN 2005)*, Montréal, Québec,
618 Canada (2005) 1722-1727.

619 Kaplan, A., Kushni, Y., Cane, M.A., & Blumenthal, M.B. (1997). Reduced space optimal
620 analysis for historical data sets: 136 years of Atlantic sea surface temperatures. *Journal of*
621 *Geographical Research*, 102 (C13), 27835-27860.

622 Koster, R.D., Dirmeyer, P.A., Guo, Z., Bonan, G., Chan, E., Cox, P., Gordon, C.T., Kanae,
623 S., Kowalczyk, E., Lawrence, D., Liu, P., Lu, C.-H., Malyshev, S., McAvaney, B., Mitchell,
624 K., Mocko, D., Oki, T., Oleson, K., Pitman, A., Sud, Y.C., Taylor, C.M., Verseghy, D., Va-
625 sic, R., Xue, Y., & Yamada, T. (2004). Regions of strong coupling between soil moisture and
626 precipitation. *Science* 20 August 2004: 305 (5687), 1138-1140, doi:10.1126/science.1100217.

627 Kusche, J. (2007). Approximate decorrelation and non-isotropic smoothing of time-variable
628 GRACE-type gravity field models. *Journal of Geodesy*, 81 (11), 733-749, doi:10.1007/s00190-
629 007-0143-3.

630 Kusche, J., Schmidt, R., Petrovic, S., & Rietbroek, R. (2009). Decorrelated GRACE time-
631 variable gravity solutions by GFZ, and their validation using a hydrological model. *Journal*
632 *of Geodesy*, 83, 903-913, doi:10.1007/s00190-009-0308-3.

633 Lebel, T., Cappelaere, B., Galle, S., Hanan, N., Kergoat, L., Levis, S., Vieux, B., Descroix,
634 L., Gosset M., Mougin, E., Peugeot, C., & Séguis, L. (2009). The AMMA-CATCH studies
635 in the Sahelian region of West-Africa: an overview. *Journal of Hydrology*, 375, 313.

636 Long, D., Scanlon, B.R., Longuevergne, L., Sun, A.Y., Fernando, D.N. & Save, H. (2013).
637 GRACE satellite monitoring of large depletion in water storage in response to the 2011
638 drought in Texas, *Geophys. Res. Lett.*, 40(13), 3395-3401, doi:10.1002/grl.50655.

639 Ljung, L. (1987). *System Identification - Theory for the User*. Prentice Hall, Englewood
640 Cliffs, N.J. 2005GL023316.

641 Mayer-Gürr, T., Eicker, A., Kurtenbach, E. (2010). ITG-GRACE 2010 unconstrained
642 monthly solutions. <http://www.igg.uni-bonn.de/apmg/>

643 Mohino, E., Rodríguez-Fonseca, B., Mechoso, C.R., Gervois, S., Ruti, P., & Chauvin, F.
644 (2011). Impacts of the tropical Pacific/Indian Oceans on the seasonal cycle of the West
645 African monsoon. *J. Clim.*, 24, 3878-3891, doi:10.1175/2011JCLI3988.1.

646 Nahmani, S., Bock, O., Bouin, M.-N., Santamaría-Gómez, A., Boy, J.-P., Collilieux, X.,
647 Métivier, L., Panet, I., Genthon, P., de Linage, C., & Wöppelmann, G. (2012). Hydrolog-
648 ical deformation induced by the West African Monsoon: Comparison of GPS, GRACE
649 and loading models. *Journal of Geophysical Research*, 117, B05409, doi:10.1029/2011
650 JB009102.

651 Nicholson, S.E. (2000). The nature of rainfall variability over Africa on time scales of
652 decades to millenia. *Global and Planetary Change* 26, 137-158.

653 Nicholson, S.E., and Coauthors (2003). Validation of TRMM and other rainfall estimates
654 with a high-density gauge dataset for West Africa. Part I: Validation of GPCC Rainfall
655 Product and Pre-TRMM Satellite and Blended Products. *Journal of Applied Meteorology*,
656 42, 1337-1354.

657 Omondi, P., Awange, J.L., Ogallo, L.A., Okoola, R.A., & Forootan, E. (2012). Decadal
658 rainfall variability modes in observed rainfall records over East Africa and their relations
659 to historical sea surface temperature changes. *Journal of Hydrology*, 464-465, 140156, doi:
660 <http://dx.doi.org/10.1016/j.jhydrol.2012.07.003>.

661 Preisendorfer, R. (1988). *Principal component analysis in Meteorology and Oceanography*.
662 Elsevier: Amsterdam, 426 pages, ISBN:0444430148.

663 Reynolds, R.W., Rayne, N.A., Smith, T.M., Stokes, D.C., & Wang, W. (2002). An im-
664 proved in situ and satellite SST analysis for climate. *J. Clim.* 15, 16091625.

665 Reager, J.T., Famiglietti, J.S. (2013). Characteristic mega-basin water storage behavior
666 using GRACE, *Water Resour. Res.*, 49, 33143329, doi:10.1002/wrcr.20264.

667 Redelsperger, J-L., Thorncroft, Ch.D., Diedhiou, A., Lebel, T., Parker, D.J., & Polcher, J.
668 (2006). African Monsoon multidisciplinary analysis: an international research project and
669 field campaign. *Bull. Amer. Meteor. Soc.*, 87, 1739-1746. doi:[http://dx.doi.org/10.1175/](http://dx.doi.org/10.1175/BAMS-87-12-1739)
670 [BAMS-87-12-1739](http://dx.doi.org/10.1175/BAMS-87-12-1739).

671 Rietbroek, R., Brunnabend, S.E., Dahle, C., Kusche, J., Flechtner, F., Schröter, J., &
672 Timmermann, R. (2009). Changes in total ocean mass derived from GRACE, GPS, and
673 ocean modeling with weekly resolution. *Journal of Geophysical Research*, 114, C11004,
674 doi:10.1029/2009JC005449.

675 Rietbroek, R., Fritsche, M., Dahle, C., Brunnabend, S-E., Behnisch, M., Kusche, J., Flecht-
676 ner, F., Schröter, J., & Dietrich, R. (2014). Can GPS-derived surface loading bridge a
677 GRACE mission gap? *Surv Geophys*, in-press, doi:10.1007/s10712-013-9276-5.

678 Rodell, M., Houser, P.R., Jambor, U., Gottschalk, J., Mitchell, K., Meng, K., Arsenault,
679 C.-J., Cosgrove, B., Radakovich, J., Bosilovich, M., Entin, J.K., Walker, J.P., Lohmann, D.,
680 & Toll, D. (2004). The Global Land Data Assimilation System. *Bulletin of the American*
681 *Meteorological Society*, 85 (3), 381-394.

682 Rodriguez-Fonseca, B., Janicot, S., Mohino, E., Losada, T., Bader, J., Caminade, C.,
683 Chauvin, F., Fontaine, B., García-Serrano, J., Gervois, S., Joly, M., Polo, I., Ruti, P.,
684 Roucou, P. & Voltaire, A. (2011). Interannual and decadal SST-forced responses of the
685 West African monsoon, *Atmos. Sci. Lett.*, 12(1), 67-74, doi:10.1002/asl.308.

686 Saji, N.H., Goswami, B.N., Vinayachandran, P. N., & Yamagata, T. (1999). A dipole mode
687 in the tropical Indian Ocean. *Nature*, 401, 360363, doi:10.1038/43854.

688 Scanlon, B.R., Faunt, C.C., Longuevergne, L., Reedy, R.C., Alley, W.M., McGuire, V.L.
689 & McMahon, P.B. (2012). Groundwater depletion and sustainability of irrigation in the
690 US High Plains and Central Valley., *Proc. Natl. Acad. Sci. U. S. A.*, 109(24), 9320-5,
691 doi:10.1073/pnas.1200311109.

692 Schmidt, R., Flechtner, F., Meyer, U., Neumayer, K.-H., Dahle, Ch., König, R., & Kusche,
693 J. (2008a). Hydrological signals observed by the GRACE satellites. *Surveys in Geophysics*,
694 29 (4-5), 319-334.

695 Schmidt, R., Petrovic, S., Güntner, A., Barthelmes, F., Wunsch, J., Kusche, J. (2008b).
696 Periodic components of water storage changes from GRACE and global hydrology models.
697 *Journal of Geophysical Research: Solid Earth*, 113:B08419.

698 Schuol, J., Abbaspour, K. C., Yang, H., Srinivasan, R. & Zehnder, A.J.B. (2008). Model-
699 ing blue and green water availability in Africa, *Water Resour. Res.*, 44, doi:10.1029/2007
700 [WR006609](http://dx.doi.org/10.1029/2007WR006609).

701 Schuol, J., & Abbaspour, K.C. (2006). Calibration and uncertainty issues of a hydrological
702 model (SWAT) applied to West Africa. *Adv. Geosci.*, 9, 137-143.

703 Speth, P., Christoph, M., & Diekkrüger, B. (2011). Impacts of global change on the hydro-
704 logical cycle in West and Northwest Africa. Speth, Peter; Christoph, Michael; Diekkrüger,
705 Bernd (Eds.). Springer Berlin Heidelberg, 675 pages. ISBN:3642129560

706 Tapley B, Bettadpur S, Watkins M, & Reigber C. (2004). The gravity recovery and cli-
707 mate experiment: Mission overview and early results. *Geophys Res Lett* 31. [http://dx.doi](http://dx.doi.org/10.1029/2004GL019920)
708 [.org/10.1029/2004GL019920](http://dx.doi.org/10.1029/2004GL019920)

709 van Dijk, A.I.J.M., Peña-Arancibia, J.L., Wood, Eric F., Sheffield, J., & Beck, H.E. (2013).
710 Global analysis of seasonal streamflow predictability using an ensemble prediction system
711 and observations from 6192 small catchments worldwide. *Water Resources Research*, 49
712 (5), 27292746, DOI: 10.1002/wrcr.20251.

713 von Storch, H., & Navarra, A. (1999). *Analysis of climate variability*. Springer, 342 p, ISBN
714 978-3-540-66315-7.

715 Wahr, J., Molenaar, M., & Bryan, F. (1998). Time variability of the Earth's gravity field:
716 Hydrological and oceanic effects and their possible detection using GRACE. *Journal of*
717 *Geophysical Research*, 103 (B12), 30205-30229, doi:10.1029/98JB02844.

718 Wang, K., & Dickinson, R.E. (2012). A review of global terrestrial evapotranspiration:
719 observation, modeling, climatology, and climatic variability. *Reviews of Geophysics*, 50
720 (2), doi:10.1029/2011RG000373.

721 Werth, S., Güntner, A., Schmidt, R., & Kusche, J. (2009a). Evaluation of GRACE filter
722 tools from a hydrological perspective. *Geophysical Journal International*, 179, 1499-1515.
723 <http://dx.doi.org/10.1111/j.1365-246X.2009.04355.x>.

724 Werth, S., Güntner, A., Petrovic, S., & Schmidt, R. (2009b). Integration of GRACE mass
725 variations into a global hydrological model. *Earth and Planetary Science Letters* 277(1),
726 166-173.

727 Westra, S., Brown, C., Lall, U., & Sharma, A. (2007). Modeling multivariable hydrological
728 series: Principal component analysis or independent component analysis? *Water Resources*
729 *Research*, 43 (6), W06429, doi:10.1029/2006WR005617.

730 Westra, S., Sharma, A., Brown, C., & Lall, U. (2008). Multivariate streamflow forecast-
731 ing using independent component analysis. *Water Resources Research*, 44 (2), W02437,
732 doi:10.1029/2007WR006104.

733 Xie, H., Longuevergne, L., Ringler, C., & Scanlon, B.R. (2012). Calibration and evaluation
734 of a semi-distributed watershed model of Sub-Saharan Africa using GRACE data, *Hydrol.*
735 *Earth Syst. Sci.*, 16(9), 3083-3099, doi:10.5194/hess-16-3083-2012.

736 Zaitchik, B.F., Rodell, M., & Reichle, R.H. (2008). Assimilation of GRACE terrestrial
737 water storage data into a land surface model: results for the Mississippi River Basin, *J.*
738 *Hydrometeor.*, 9 (3), 535-548, doi:10.1175/2007JHM951.1.

739 Appendix A (Computational Details of Total Water Storage Fields)

740 In order to prepare the data sets for analysis, the following processing steps were
741 applied.

- 742 – The GRACE Level-2 data that are used here, are derived in terms of fully nor-
743 malized spherical harmonic (SH) coefficients of the geopotential fields (Flecht-
744 ner, 2007). Firstly, the fields were augmented by the degree-1 term from Ri-
745 etbroek et al. (2009) in order to include the variation of the Earth’s center of
746 mass with respect to a crust-fixed reference system.
- 747 – GRACE SHs at higher degrees are affected by correlated noise and are, there-
748 fore, smoothed by applying the DDK2 decorrelation filter (Kusche et al., 2009).
749 Werth et al. (2009a) found that the DDK2-filtered GRACE solutions are gener-
750 ally in good agreement with the output of global hydrological models. How-
751 ever, GRACE solutions are also contaminated by errors due to incomplete
752 reduction of short-term mass variations by de-aliasing models (Forootan et al.,
753 2013, 2014). We found that the impact of atmospheric de-aliasing errors on the
754 GRACE-derived TWS over West Africa is negligible (see atmospheric errors
755 over the Niger Basin in Forootan et al., 2014).
- 756 – GRACE DDK2 filtered solutions up to degree and order 120 were then used
757 to generate the global TWS values according to the approach of Wahr et al.
758 (1998).
- 759 – Similar to the GRACE products above, the DDK2 filter was applied to the
760 gridded WGHM-TWS data set in order to preserve exactly the same spectral
761 content as with the filtered GRACE products.
- 762 – After filtering, all data sets were converted to $0.5^\circ \times 0.5^\circ$ grids similar to the
763 WGHM-TWS outputs.
- 764 – From each data set, a rectangular region that includes West Africa (latitude
765 between 0° to $25^\circ N$ and longitude between -20° to $10^\circ E$) was selected.

766 Lake Volta (see Fig. A1) is one of the largest man-made reservoirs in the world,
767 created by the Akosombo Dam, which holds back the water for generating hydro-
768 electric power (for details see Speth et al., 2011). Satellite altimetry observations
769 indicate a sharp increase of water level since mid 2007, where much of the excess
770 water resulted from heavy rainfall within the catchment (Crétaux et al., 2011).
771 This introduces an artificial TWS anomaly located over the lake, which is removed
772 to avoid its misinterpretation as a part of subsurface TWS changes. The equivalent
773 water height (EWH) change of Volta was computed by assuming a grid mask
774 representing a unit change in EWH of 1 mm over the entire lake surface and zero
775 elsewhere. The grid mask has been converted into a set of spherical harmonic
776 coefficients up to degree 120 and subsequently filtered using the same DDK2 filter
777 used for filtering the original GRACE-TWS data. Then, each field was scaled
778 using the lake height time-series (in mm) derived from the results of Crétaux et al.
779 (2011). The averaged storage changes derived from GRACE-TWS (from GFZ) and
780 altimetry are shown in Fig. A1. Both altimetry and GRACE GFZ-TWS indicate
781 an increase of water storage within the lake. The amplitude of the signal derived
782 from GRACE GFZ-TWS is larger than that of the altimetry likely since GRACE-
783 TWS also reflects the groundwater signal of the surrounding area of the lake. For
784 the lake area, we estimate a TWS increase of $2.95 \pm 1.32 \text{ km}^3 \cdot \text{yr}^{-1}$, during 2003

785 to 2010. The time series of Lake Volta water storage changes were then removed
786 from GRACE-TWS fields (including both GFZ and ITG2010).

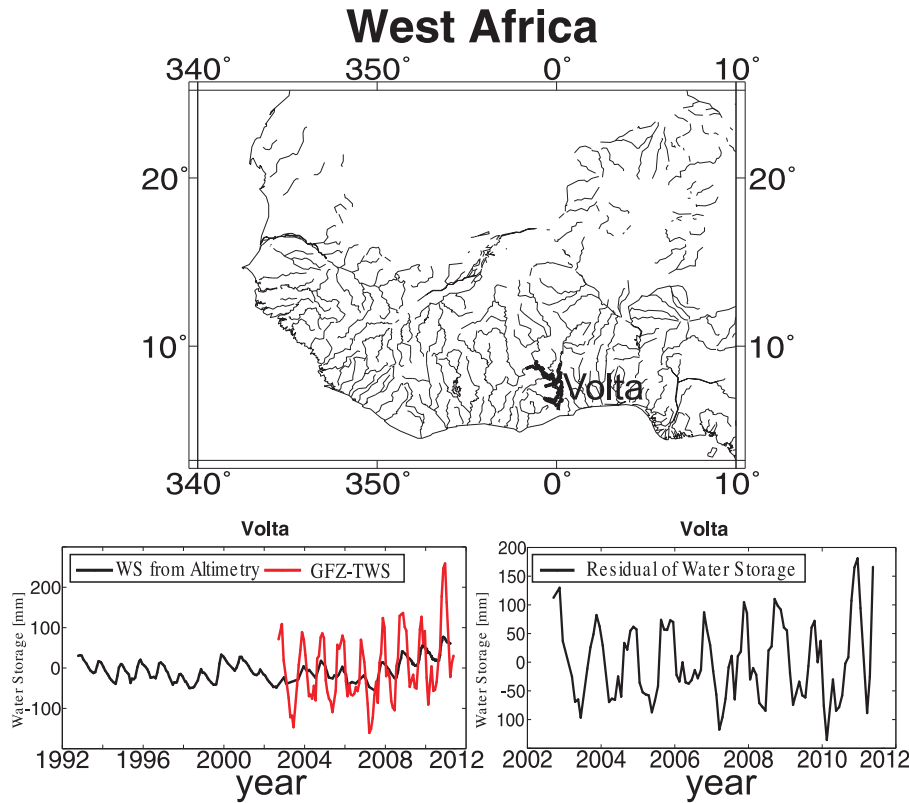


Figure A1: Overview of water storage changes of Volta Lake. The graph on top shows the location of the lake, while that of the bottom-left compares the averaged contribution of Volta lake level changes (derived from altimetry in black) with the averaged TWS variations derived from GRACE (GFZ-TWS products, in red). The bottom-right graph shows the GRACE GFZ-TWS signal after removing the water storage signal of Lake Volta.

787 In order to compare the signal strength over the region, the signal root-mean-
788 square value (RMS) and the linear trend of the three mentioned TWS data sets
789 (GFZ, ITG2010 and WGHM) are computed for the period January 2003 to August
790 2009, in which the three data sets were available (see Fig. A2). From the RMS, one
791 concludes that all the three data sets show a strong variability over the tropical
792 and the Gulf of Guinea coastal regions. The computed linear trends, however,
793 are not consistent. Particularly, GRACE-derived TWS changes show a mass gain
794 over Volta Lake, which we remove from the GRACE-TWS fields before performing
795 decomposition. Removing such artificial anomaly is necessary, since otherwise the
796 amplitude of TWS forecast over the lake will be overestimated.

Results for the period January 2003 to August 2009

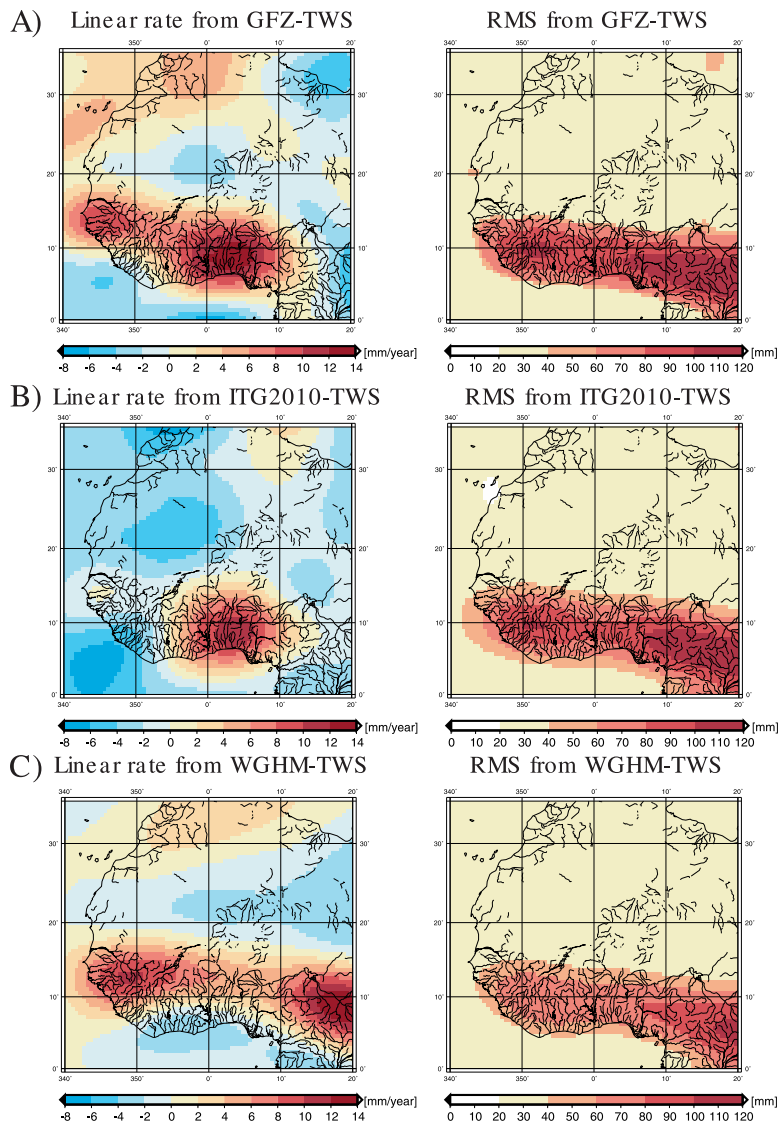


Figure A2: Comparing the signal variability (RMS) and linear trends of TWS data used in this study after smoothing using the Kusche et al. [2009]'s DDK2 filter. (A) TWS data of GRACE GFZ RL04, (B) TWS data of GRACE ITG2010, and (C) TWS of WGHM.

797 **Appendix B (Details of ICA and ARX Methods)**

798 This appendix provides details of computations regarding to the methodology
799 described in Section 3.

801 ICA decomposition is performed here by applying a 2-step algorithm (Forootan
 802 and Kusche, 2012) on the available data sets, where step 1 consists of data decor-
 803 relation using principal component analysis (PCA). In step 2, the j -dominant
 804 components of PCA are rotated to be as independent from each other as possible.
 805 Storing the available data in a $n \times p$ data matrix \mathbf{X} , after removing their temporal
 806 mean, where n is the number of months and p is the number of grid points, ICA
 807 decomposes \mathbf{X} as

$$\mathbf{X} \simeq \mathbf{X}_j = \bar{\mathbf{P}}_j \mathbf{R}_j \mathbf{\Lambda}_j \mathbf{R}_j^T \bar{\mathbf{E}}_j^T. \quad (\text{B1})$$

808 In Eq. (B1), $\bar{\mathbf{P}}_j \mathbf{\Lambda}_j \bar{\mathbf{E}}_j^T$ is derived from the PCA decomposition of \mathbf{X} in step 1.
 809 Therefore, $\mathbf{\Lambda}_j$ is an $j \times j$ diagonal matrix that stores the singular values arranged
 810 with respect to the magnitude, $\bar{\mathbf{E}}_j$ ($j \times p$) contains the corresponding unit-length
 811 spatial eigenvectors, $\bar{\mathbf{P}}_j$ ($n \times j$) contains the associated normalized temporal com-
 812 ponents, and $j < n$ is the number of retained dominant modes (Preisendorfer,
 813 1988). The orthogonal rotation matrix \mathbf{R}_j ($j \times j$) is defined in step 2, so that it
 814 rotates PCs and make them as statistically independent as possible. The method
 815 equals to temporal ICA (Forootan and Kusche, 2012), which is simply called ICA
 816 in the paper. Considering Eqs. (1) and (2), \mathbf{Y} and \mathbf{U} are equivalent to $\bar{\mathbf{P}}\mathbf{R}$, while
 817 \mathbf{A} and \mathbf{B} are equivalent to $\mathbf{\Lambda}\bar{\mathbf{E}}\mathbf{R}$. An optimum \mathbf{R} was found by digonalization
 818 of the fourth-order cross cumulants of the dominant temporal components $\bar{\mathbf{P}}$ (see
 819 details in Forootan and Kusche, 2012).

820 For properly selecting the subspace dimension j or j' , we used a Monte Carlo
 821 approach which simulates data from a random distribution $\mathbf{N}(\mathbf{0}, \mathbf{\Sigma})$, with $\mathbf{\Sigma}$
 822 containing the column variance of \mathbf{X} . The null hypothesis is that \mathbf{X} is drawn from
 823 such a distribution (see also Preisendorfer, 1988, pages 199 to 205). To apply
 824 the rule, 100 time series realizations of $\mathbf{N}(\mathbf{0}, \mathbf{\Sigma})$ are generated, their eigenvalues
 825 computed and placed in decreasing order. The 95th and 5th percentile of the cum-
 826 ulative distribution are then plotted (red lines in Fig. B1). Eigenvalues from the
 827 actual data sets that are above the derived confidence boundaries are unlikely to
 828 result from a data set consisting of only noise. To estimate the uncertainties of
 829 the eigenvalues, we randomly selected a subsample of \mathbf{X} and applied PCA, then
 830 selected another subsample and repeated this operation 200 times. This approach
 831 follows the ‘bootstrapping’ method as presented, e.g., in Efron (1979) and yields
 832 uncertainty estimates (see error-bars in Fig. B1). The repeat number of 200 is cho-
 833 sen experimentally to be sure that the distribution of the estimated eigenvalues is
 834 independent from the selections of the subsamples.

835 To illustrate what we describe above, Fig. B1 shows the eigenvalue spectrum of
 836 the centered time series of GRACE GFZ-derived TWS, SST and rainfall computed
 837 using PCA. The significance levels are shown by red lines and the error-bars show
 838 the uncertainties of eigenvalues. The eigenvalues above the red lines are statistically
 839 significant. The significant eigenvalues along with their orthogonal components are
 840 rotated towards independence using Eq. (B1) and interpreted in Section 4.

841 Based on the uncertainties of the PCA results (Fig. B1), in order to estimate the
 842 uncertainty of the ICs (Eq. (B1)), we generated 100 realizations of \mathbf{X} , reconstructed
 843 by $\bar{\mathbf{P}}_j$, $\mathbf{\Lambda}_j$, and $\bar{\mathbf{E}}_j$ along with 100 realizations of their errors. Then, applying Eq.

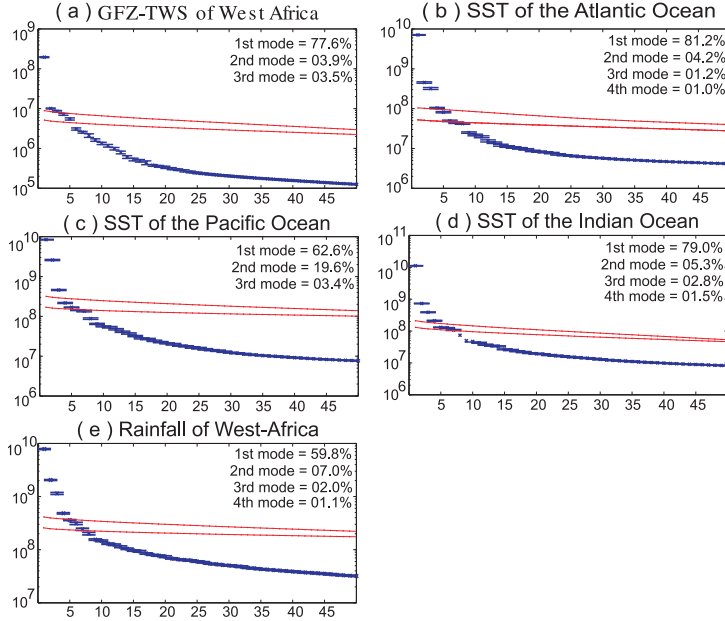


Figure B1: Eigenvalue results derived from implementing the PCA method on (a) time series of GRACE GFZ-TWS maps, (b) maps of SST over the Atlantic, (c) maps of SST over the Pacific, (d) maps of SST over the Indian Ocean basins, and (e) West-African rainfall maps from TRMM. Uncertainties are shown by error-bars around each eigenvalues. The red lines correspond to the significant test, described in Appendix B. The variance fractions of the dominant eigenvalues are represented in each graph.

844 (B1) to the realizations allows the estimation of uncertainties (see, e.g., error-bars
845 in Figs. 1, 2, and 3).

846 The projection of the data \mathbf{X} onto the i 'th spatial pattern of the ICA $\hat{\mathbf{p}}_i = \mathbf{X}\hat{\mathbf{e}}_i$,
847 provides its corresponding temporal evolution

$$\hat{\mathbf{p}}_i(t) = \sum_{s=1}^p x(t, s) \hat{\mathbf{e}}_i(s), \quad (\text{B2})$$

848 where t is time $(1, \dots, n)$ and s is the number of grid points $(1, \dots, p)$.

849 The ARX Computations

850 Considering Eq. (3) as the ARX model, the ARX-forecast requires two steps:
851 (i) The coefficients (a_1, \dots, a_{n_a}) and $(b_{q,1}, b_{q,2}, \dots, b_{q,n_b}), q = 1, \dots, m$ are es-
852 timated, e.g., using a least squares approach. This step is usually referred to as
853 'simulation' or 'training step' in literature (see, e.g., Ljung, 1987). Step (i) is per-
854 formed under the assumption that the output and inputs up to the time $t = t_n - 1$
855 are known. Furthermore, the outputs and exogenous values on the right hand side

856 of Eq. (3) are not stochastic. To avoid negative indices, one might consider the ob-
 857 servations $\mathbf{y}(t) = [y(t), y(t-1), \dots, y(c)]^T$, where $c = \max(n_a, n_b) + \max(k_q) + 1$.
 858 Eq. (3) is expanded as

$$\mathbf{y} = \begin{bmatrix} -y(t-1) & \cdots & -y(t-n_a) & u_q(t-k_q) & \cdots & u_q(t-k_q-n_b+1) \\ -y(t-2) & \cdots & -y(t-n_a-1) & u_q(t-k_q-1) & \cdots & u_q(t-k_q-n_b) \\ \vdots & \vdots & \vdots & \vdots & \vdots & \vdots \\ -y(c-1) & \cdots & -y(c-n_a) & u_q(c-k_q) & \cdots & u_q(c-k_q-n_b+1) \end{bmatrix} \begin{bmatrix} a_1 \\ \vdots \\ a_{n_a} \\ b_{q,1} \\ \vdots \\ b_{q,n_b} \end{bmatrix} + \boldsymbol{\Xi}(t), \quad (\text{B3})$$

859 where $q = 1, \dots, m$ and $\boldsymbol{\Xi}(t) = [\xi(t), \xi(t-1), \dots, \xi(c)]^T$. Eq. (B3) can be re-
 860 written compactly as

$$\mathbf{y}(t) = \boldsymbol{\Phi}(t)\boldsymbol{\Theta} + \boldsymbol{\Xi}(t). \quad (\text{B4})$$

861 The least squares estimation of the unknown coefficients is derived from

$$\hat{\boldsymbol{\Theta}} = \left(\boldsymbol{\Phi}(t)^T \boldsymbol{\Phi}(t) \right)^{-1} \boldsymbol{\Phi}(t)^T \mathbf{y}(t). \quad (\text{B5})$$

862 The quality of the fit (η) can be assessed by computing the signal-to-noise ratio
 863 as

$$\eta = 1 - \frac{\mathbf{y}(t)^T \boldsymbol{\Phi}(t) \hat{\boldsymbol{\Theta}}}{\mathbf{y}(t)^T \mathbf{y}(t)}. \quad (\text{B6})$$

864 The residual of the ARX model ($\hat{\boldsymbol{\Xi}}(t) = [\hat{\xi}(t), \hat{\xi}(t-1), \dots, \hat{\xi}(c)]^T$) can be estimated
 865 as

$$\hat{\boldsymbol{\Xi}}(t) = \mathbf{y}(t) - \boldsymbol{\Phi}(t) \hat{\boldsymbol{\Theta}}. \quad (\text{B7})$$

866 In step (ii), based on $\hat{\boldsymbol{\Theta}} = [\hat{a}_1 \dots \hat{a}_{n_a} \hat{b}_{q,1} \hat{b}_{q,2} \dots \hat{b}_{q,n_b}]^T$, when the inputs $u_q(t)$
 867 are known, one can forecast the output $\hat{y}(t_n)$ at time t_n using

$$\hat{y}(t_n) = - \sum_{i=1}^{n_a} \hat{a}_i y(t_n - i) + \sum_{q=1}^m \sum_{l=1}^{n_b} \hat{b}_{q,l} u_q(t_n - k_q - (l-1)). \quad (\text{B8})$$

868 To estimate the uncertainty of the ARX simulation, using Monte Carlo sampling,
 869 we numerically generate several realizations of the ICs (described before). By in-
 870 serting them into Eq. (3) and fitting ARX models, we are able to perform an error
 871 assessment of the fitted model up to the time t_n . For error estimation of the fore-
 872 cast (the ARX value at the time $t_n + 1$ and later), however, one should compute
 873 an accumulated error, since there is no observed value for the output y at time
 874 $t_n + 1$ and later.